

Electronic Supplementary Information

**A four-parameter system for rationalising the electronic properties of  
transition metal-radical ligand complexes**

Nicole M. Mews,<sup>a</sup> Marc Reimann,<sup>b</sup> Gerald Hörner,<sup>c</sup> Martin Kaupp,<sup>b</sup> Hartmut Schubert<sup>a</sup>  
and Andreas Berkefeld\*<sup>a</sup>

<sup>a</sup> Institut für Anorganische Chemie, Eberhard Karls Universität Tübingen, Auf der Morgenstelle 18,  
72076 Tübingen, Germany

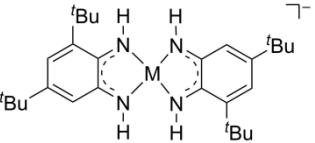
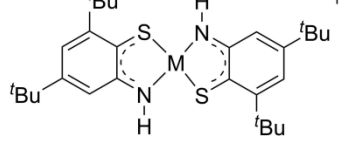
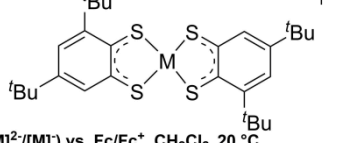
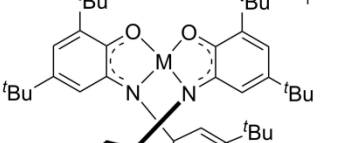
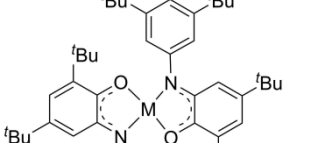
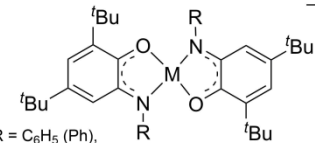
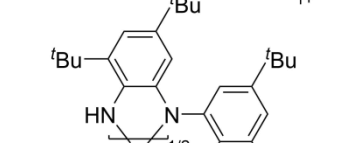
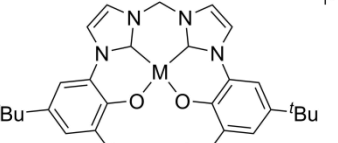
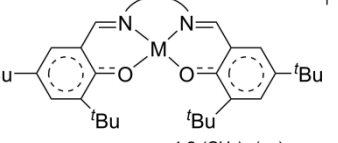
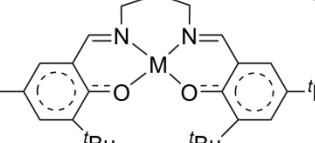
<sup>b</sup> Institut für Chemie, Theoretical Chemistry–Quantum Chemistry, Technische Universität Berlin,  
Straße des 17. Juni 135, 10623 Berlin, Germany

<sup>c</sup> Anorganische Chemie IV, Universität Bayreuth, Universitätsstraße 35, 95440 Bayreuth, Germany

**Table of Contents**

1	Additional Information on Group 10 Metal Radical-Ligand Coordination Compounds.....	2
2	General Information.....	3
3	Synthetic Procedures and Analytical Data.....	5
4	Additional Solid-State Structure Data .....	10
5	Additional NMR Spectroscopic Data .....	12
6	Additional Information on UV/Vis/NIR Spectroscopy Data.....	13
7	Additional X-Band cw-EPR Data.....	19
8	Additional Electrochemical Data.....	26
9	Additional Computational Data .....	30
9.1	General Information .....	30
9.2	Computational Results .....	31
10	References .....	35

# 1 Additional Information on Group 10 Metal Radical-Ligand Coordination Compounds

 <p><math>E([M]^{2+}/[M]^+)</math> vs. <math>Fc/Fc^+</math>, MeCN, 20 °C Pt &lt; Ni &lt; Pd -2.22 -2.12 -1.86 V</p> <p>UV/vis/NIR, MeCN, 20 °C: <math>\lambda_{max}</math> (E/kJ mol<sup>-1</sup>) Pt &lt; Ni &lt; Pd 918 (130) 1031 (116) 1232 nm (97)</p> <p>EPR (X-Band): MeCN, 30 K (Ni, Pt), 10 K (Pd) <math>g_{iso}</math>: Pd &lt; Pt &lt; Ni 2.008 2.0165 2.0333 <math>\Delta g</math>: Pd &lt; Ni = Pt 0.038 0.105 0.108</p> <p>Calculated spin density at M not reported <i>J. Am. Chem. Soc.</i> <b>2003</b>, 125, 9116</p>	 <p><math>E([M]^{2+}/[M]^+)</math> vs. <math>Fc/Fc^+</math>, CH<sub>2</sub>Cl<sub>2</sub>, 22 °C Ni &lt; Pt &lt; Pd -1.714 -1.527 -1.484 V</p> <p>UV/vis/NIR, CH<sub>2</sub>Cl<sub>2</sub>, -40 °C: <math>\lambda_{max}</math> (E/kJ mol<sup>-1</sup>) Ni = Pt 971 (123) 980 nm (122)</p> <p>EPR (X-Band): CH<sub>2</sub>Cl<sub>2</sub>, 10 K <math>g_{iso}</math>: Pt &lt; Ni 2.021 2.067 <math>\Delta g</math>: Ni = Pt 0.109 0.378</p> <p>Calculated spin density at M not reported <i>J. Am. Chem. Soc.</i> <b>2001</b>, 123, 10012</p>	 <p><math>E([M]^{2+}/[M]^+)</math> vs. <math>Fc/Fc^+</math>, CH<sub>2</sub>Cl<sub>2</sub>, 20 °C Ni = Pt &lt; Pd -1.10 -1.10 -0.92 V</p> <p>UV/vis/NIR, CH<sub>2</sub>Cl<sub>2</sub>, 20 °C: <math>\lambda_{max}</math> (E/kJ mol<sup>-1</sup>) Ni = Pt &lt; Pd 890 (134) 900 (133) 1140 nm (105)</p> <p>EPR (X-Band): CH<sub>2</sub>Cl<sub>2</sub> (Pd, Pt), DMF/CHCl<sub>3</sub> (Ni), 10 K <math>g_{iso}</math>: Pd = Pt &lt; Ni 2.02 2.02 2.077 <math>\Delta g</math>: Pd &lt; Ni &lt; Pt 0 0.17 0.41</p> <p>Calculated spin density at M Pd &lt; Pt &lt; Ni 21 24 34 % <i>Inorg. Chem.</i> <b>2005</b>, 44, 5345</p>	 <p><math>E([M]^{2+}/[M]^+)</math> vs. <math>Fc/Fc^+</math>, CH<sub>2</sub>Cl<sub>2</sub> Pt &lt; Ni &lt; Pd -1.65 -1.59 -1.43 V</p> <p>UV/vis/NIR, CH<sub>2</sub>Cl<sub>2</sub>: <math>\lambda_{max}</math> (E/kJ mol<sup>-1</sup>) Pt &lt; Ni &lt; Pd 1262 (95) 1515 (79) 1661 nm (72)</p> <p>EPR data: not reported Calculated spin density at M not reported <i>Inorg. Chem.</i> <b>2018</b>, 57, 3272</p>	 <p><math>E([M]^{2+}/[M]^+)</math> vs. <math>Fc/Fc^+</math>, CH<sub>2</sub>Cl<sub>2</sub> Ni = Pt &lt; Pd -1.91 -1.91 -1.67 V</p> <p>UV/vis/NIR, CH<sub>2</sub>Cl<sub>2</sub>: <math>\lambda_{max}</math> (E/kJ mol<sup>-1</sup>) Pt &lt; Ni &lt; Pd 1105 (108) 1321 (91) 1547 nm (77)</p> <p>EPR data: not reported Calculated spin density at M not reported <i>Inorg. Chem.</i> <b>2018</b>, 57, 3272</p>
 <p>R = C<sub>6</sub>H<sub>5</sub> (Ph), o-CF<sub>3</sub>-C<sub>6</sub>H<sub>4</sub> (Ph<sup>h</sup>)</p> <p><math>E([M]^{2+}/[M]^+)</math> vs. <math>Fc/Fc^+</math>, CH<sub>2</sub>Cl<sub>2</sub>, 298 K Ni (R = Ph) = Pt<sup>a</sup> (R = Ph) &lt; Pd<sup>b</sup> (R = Ph) -1.64 -1.64 -1.54 V</p> <p>UV/vis/NIR, CH<sub>2</sub>Cl<sub>2</sub>, 25 °C: <math>\lambda_{max}</math> (E/kJ mol<sup>-1</sup>) Ni (R = Ph) &lt; Pt<sup>a</sup> (R = Ph) &lt; Pd<sup>b</sup> (R = Ph) 890 (134) 1059 (113) 1564 nm (76)</p> <p>EPR (X-Band): CH<sub>2</sub>Cl<sub>2</sub>, 10 K <math>g_{iso}</math>: Pd<sup>b</sup> (R = Ph) &lt; Pt<sup>a</sup> (R = Ph) 2.021 2.036 <math>\Delta g</math>: Pd<sup>b</sup> (R = Ph) &lt; Pt<sup>a</sup> (R = Ph) 0.0975 0.361</p> <p>Calculated spin density at M Pt<sup>a</sup> (R = Ph) = 23.7 % <i>J. Am. Chem. Soc.</i> <b>2001</b>, 123, 2213 <sup>a</sup><i>Inorg. Chem.</i> <b>2002</b>, 41, 4295 <sup>b</sup><i>Inorg. Chem.</i> <b>2005</b>, 44, 3709</p>	 <p><math>E([M]^{2+}/[M]^+)</math> vs. <math>Fc/Fc^+</math>, CH<sub>2</sub>Cl<sub>2</sub>, 298 K Pd &lt; Ni &lt; Pt -0.38 -0.31 -0.25 V</p> <p>UV/vis/NIR, CH<sub>2</sub>Cl<sub>2</sub>, 298 K: <math>\lambda_{max}</math> (E/kJ mol<sup>-1</sup>) Pt &lt; Ni &lt; Pd 1248 (96) 1536 (78) 1644 nm (73)</p> <p>EPR (X-Band): solid-state, 100 K <math>g_{iso}</math>: Pd = Ni &lt; Pt 1.992 1.992 1.978 <math>\Delta g^a</math>: Pd = Ni &lt; Pt 0.007 0.008 0.025</p> <p>a) <math>\Delta g = g_{(lowest\ field)} - g_{iso}</math> Calculated spin density at M not reported <i>Eur. J. Inorg. Chem.</i> <b>2018</b>, 1752</p>	 <p><math>E([M]^{2+}/[M]^+)</math> vs. <math>Fc/Fc^+</math>, CH<sub>2</sub>Cl<sub>2</sub>, 298 K Ni &lt; Pd = Pt 0.11 0.21 0.21 V</p> <p>UV/vis/NIR, CH<sub>2</sub>Cl<sub>2</sub>, 298 K: <math>\lambda_{max}</math> (E/kJ mol<sup>-1</sup>) Pt &lt; Ni &lt; Pd 2294 (52) 2390 (50) 2600 nm (46)</p> <p>EPR (X-Band): solid-state, 100 K <math>g_{iso}</math>: Pd &lt; Ni &lt; Pt 2.004 2.032 2.044 <math>\Delta g^a</math>: Pd &lt; Ni &lt; Pt 0.017 &lt; 0.055 &lt; 0.096</p> <p>a) <math>\Delta g = g_{(lowest\ field)} - g_{iso}</math> Calculated spin density at M: B3LYP-D3/6-31g*/LANL2DZ ECP (for M) Pd &lt; Ni = Pt (Mulliken) 0.04 0.07 0.07 <i>Inorg. Chem.</i> <b>2019</b>, 58, 8030</p>	 <p><math>\cap = 1,2-(CH_2)_2</math> (en), 1,2-cyclo-C<sub>6</sub>H<sub>10</sub> (cy)</p> <p><math>E([M]^{2+}/[M]^+)</math> vs. <math>Fc/Fc^+</math>, CH<sub>2</sub>Cl<sub>2</sub>, 230 K Pt(<math>\cap</math> = en) &lt; Ni(<math>\cap</math> = cy) &lt; Pd(<math>\cap</math> = cy) 0.35 0.37 0.45 V</p> <p>UV/vis/NIR, CH<sub>2</sub>Cl<sub>2</sub>, 298 K: <math>\lambda_{max}</math> (E/kJ mol<sup>-1</sup>) Pt(<math>\cap</math> = en) &lt; Ni(<math>\cap</math> = cy) &lt; Pd(<math>\cap</math> = cy) 1834 (65) 2127 (56) 2439 nm (49)</p> <p>EPR (X-Band)<sup>a</sup>: solid-state, 77 K <math>g_{iso}</math>: Pd(<math>\cap</math> = cy) &lt; Pt(<math>\cap</math> = en) &lt; Ni(<math>\cap</math> = cy) 2.01 2.03 2.06 <math>\Delta g</math>: Pd(<math>\cap</math> = cy) &lt; Ni(<math>\cap</math> = cy) &lt; Pt(<math>\cap</math> = en) 0 0.16 0.56</p> <p>Calculated spin density at M Pd(<math>\cap</math> = cy) &lt; Ni(<math>\cap</math> = cy) &lt; Pt(<math>\cap</math> = en) 8 12 17 % <i>Inorg. Chem.</i> <b>2009</b>, 48, 8383 <sup>a</sup><i>J. Am. Chem. Soc.</i> <b>2007</b>, 129, 2559</p>	 <p><math>E([M]^{2+}/[M]^+)</math> vs. <math>Fc/Fc^+</math>, CH<sub>2</sub>Cl<sub>2</sub>, 230 K Ni = Pt &lt; Pd 0.43 0.44 0.52 V</p> <p>UV/vis/NIR, CH<sub>2</sub>Cl<sub>2</sub>, 298 K: <math>\lambda_{max}</math> (E/kJ mol<sup>-1</sup>) Pt &lt; Ni &lt; Pd 1996 (60) 2325 (51) 2531 nm (47)</p> <p>EPR (X-Band): CH<sub>2</sub>Cl<sub>2</sub>, 20 K <math>g_{iso}</math>: Pd &lt; Ni &lt; Pt 2.007 2.040 2.045 <math>\Delta g</math>: Pd &lt; Ni &lt; Pt 0 0 0.48</p> <p>Calculated spin density at M Ni = Pd &lt; Pt 7 7 16 % <i>Dalton Trans.</i> <b>2011</b>, 40, 2469</p>

**Fig S1** Compilation of properties of representative radical-ligand complexes of group 10 metals (from left to right): top row, entry no. 1,<sup>1</sup> 2,<sup>2</sup> 3,<sup>3</sup> 4 and 5;<sup>4</sup> bottom row, entry no. 1,<sup>5-7</sup> 2,<sup>8</sup> 3,<sup>9</sup> 4,<sup>10,11</sup> and 5<sup>12</sup>.

## 2 General Information

All manipulations of air- and moisture sensitive compounds were carried out under an atmosphere of dry argon using standard Schlenk or glove box techniques. Literature procedures were followed for the preparation of 5',5'''-di-tert-butyl-2,2''',4,4''',6,6'''-hexamethyl-[1,1':3',1'':4'',1'''':3''',1''''-quinquephenyl]2',2'''-dithiol ( $\text{Mes}_2^t\text{Bu}_2(\text{SH})_2$ ),  $^{\text{Mes}}\text{Ni-PCy}_3$ ,<sup>13</sup> *trans*-py<sub>2</sub>PtCl<sub>2</sub>,<sup>14</sup> *trans*-py<sub>2</sub>PdCl<sub>2</sub>,<sup>15</sup>  $[(\eta^5\text{-}(\text{MeC}(\text{O})\text{C}_5\text{H}_4)_2\text{Fe})\text{N}(\text{SO}_2\text{CF}_3)_2]$ ,<sup>16</sup>  $[(4\text{-BrC}_6\text{H}_4)_3\text{N}]\text{BAr}^{\text{F}_4}$  ( $\text{BAr}^{\text{F}_4} = (3,5\text{-}(\text{F}_3\text{C})_2\text{C}_6\text{H}_3)_4\text{B}^-$ ),<sup>17</sup> benzyl potassium,<sup>18</sup> and 1,4-bis(4,6-di-tert-butylthiophenol-2-yl)benzene ( $^t\text{Bu}_4(\text{SH})_2$ ).<sup>19</sup>

AgClO<sub>4</sub> (Alfa Aesar), 1,1'-diacetylferrocene (TCI), PPh<sub>3</sub> and PCy<sub>3</sub> (abcr) were used as received. High purity ferrocene (Fc, 99.5 %; TCI) was sublimed, and stored under argon. In general, solvents were purified and dried prior to use. Propylene carbonate (PC) was pre-dried and purified by fractional distillation under reduced pressure and percolation through a column of activated neutral alumina. 1,1,2,2-C<sub>2</sub>H<sub>2</sub>Cl<sub>4</sub> was dried over and distilled from P<sub>2</sub>O<sub>5</sub> and degassed. Pentane and toluene were pre-dried over activated 3 Å molecular sieves (MS) and distilled from sodium benzophenone ketyl under argon. Et<sub>3</sub>N was distilled from and stored over 3 Å MS. Dichloromethane stabilized with EtOH (CHEMSOLUTE, Th. Geyer) was first distilled from P<sub>2</sub>O<sub>5</sub>, then from K<sub>2</sub>CO<sub>3</sub>, and finally stored over activated basic alumina. Acetonitrile (MeCN) for use in electrochemical experiments was sequentially dried over and distilled from CaH<sub>2</sub> and P<sub>2</sub>O<sub>5</sub>, and finally percolated through activated neutral alumina. 1,2-Difluorobenzene (1,2-C<sub>6</sub>H<sub>4</sub>F<sub>2</sub>; abcr) was dried and purified by percolation through a column of activated neutral alumina, and distilled onto activated neutral alumina prior to use. C<sub>6</sub>D<sub>6</sub> was dried over and distilled from NaK alloy. CD<sub>2</sub>Cl<sub>2</sub> and CDCl<sub>3</sub> were dried over and vacuum transferred from 3 Å MS. In general, solvents were stored over 3 Å MS under argon. Molecular sieves and alumina were activated by heating under dynamic vacuum (10<sup>-3</sup> mbar) at  $T \leq 200$  °C for 24-48 h.

NMR data were acquired on a Bruker Avance III HDX 600 and an AVII+500 spectrometer (DOSY). <sup>1</sup>H and <sup>13</sup>C{<sup>1</sup>H}-NMR chemical shifts are referenced to the residual proton and naturally abundant carbon resonances of the solvents: 7.16/128.06 (C<sub>6</sub>D<sub>6</sub>), 5.32/53.84 (CD<sub>2</sub>Cl<sub>2</sub>), 7.26/77.16 (CDCl<sub>3</sub>). <sup>31</sup>P NMR chemical shifts are referenced to an external standard sample of 85 % H<sub>3</sub>PO<sub>4</sub> set to 0 ppm. <sup>195</sup>Pt NMR chemical shifts are referenced to an external standard sample of 1.2 M hexachloroplatinate(IV) in D<sub>2</sub>O set to 0 ppm.

EPR spectra were collected using 4 mm O.D. Wilmad quartz (CFQ) EPR tubes or 5 mm O.D. NMR tubes on a continuous wave X-band Bruker EMXmicro spectrometer, and are referenced to the Bruker Strong Pitch standard  $g_{\text{iso}} = 2.0028$ . EPR simulations were done with EasySpin (version 5.1.25)<sup>20</sup> and MATLAB and Statistic Toolbox Release R2016a (The MathWorks, Inc., Natick, Massachusetts, United States). X-band cw-EPR spectral data were fitted using the easyfit tool included in EasySpin package (pepper for solid state and garlic for solution data).

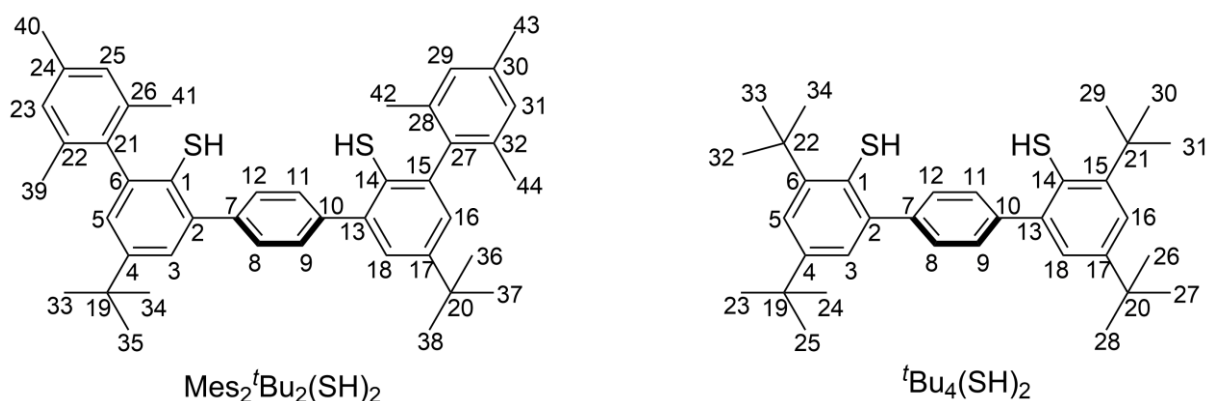
In general, the sample concentrations for electronic spectra were corrected for temperature dependent changes of solvent density  $\rho$  by using a modified form of the Rackett equation.<sup>21, 22</sup>

Evan's method<sup>23</sup> was employed to determine  $\mu_{\text{eff}}$  in solution using a coaxial insert for 5 mm NMR sample tubes,  $\chi_{\text{M}}^{\text{dia}} = -0.5 \times M$ ,  $M$  = dimensionless molecular weight of the sample and  $\chi_{\text{M}}^{\text{dia}}(\text{CD}_2\text{Cl}_2) = -4.66 \times 10^{-5} \text{ cm}^3 \text{ mol}^{-1}$  were used to correct for diamagnetic susceptibilities of sample and solvent.<sup>24</sup>

X-Ray diffraction data were collected on a Bruker Smart APEXII diffractometer with graphite-monochromated  $\text{MoK}_\alpha$  radiation. The programs used were Bruker's APEX2 v2011.8-0, including SADABS for absorption correction and SAINT for structure solution, the WinGX suite of programs version 2013.3,<sup>25</sup> SHELXS and SHELXL for structure solution and refinement,<sup>26, 27</sup> PLATON,<sup>28</sup> and ORTEP.<sup>29</sup> Crystals were, unless otherwise noted, coated in a perfluorinated polyether oil and mounted on a 100  $\mu\text{m}$  MiTeGen MicroMounts™ loop that was placed on the goniometer head under a stream of dry nitrogen at 100 K.

Cyclic voltammetry (CV) measurements were performed under argon at 17 °C using a Julabo CF40 (resistance thermometer: Pt-100, temperature range: -40 to 50 °C) and an ECi 200 potentiostat (Nordic Electrochemistry) and BASi CV-50W voltammetric analyzer (Bioanalytical Systems, Inc.) in a gas-tight, full-glass, three-electrode cell setup. The ECi 200 potentiostat was controlled by using the EC4 DAQ (version 4.1.133.1, Nordic Electrochemistry) software, and data were treated with EC4 VIEW (version 1.2.55.1, Nordic Electrochemistry).  $n\text{Bu}_4\text{NPF}_6$  electrolyte (Alfa Aesar) was recrystallized 3 times from acetone/water and employed as a 0.1 M solution in  $\text{CH}_2\text{Cl}_2$  and MeCN. A Pt disc electrode (Deutsche Metrohm GmbH & Co. KG, electro-active area =  $0.080 \pm 0.003 \text{ cm}^2$ ) and a 1 mm coiled Pt-wire were employed as working and counter electrodes. The  $\text{Ag}/\text{Ag}^+$  redox couple, in the form of a 0.5 mm Ag wire in a 0.01 M  $\text{AgClO}_4/0.1 \text{ M } n\text{Bu}_4\text{NPF}_6$  MeCN solution, served as a reference electrode. Cyclic voltammograms were corrected for capacitive currents of electrolyte solutions and overall cell resistance, and potentials are reported relative to  $\text{Fc}/[\text{Fc}]^+$  in  $\text{CH}_2\text{Cl}_2$ , with  $E^0(\text{Fc}/[\text{Fc}]^+/0.1 \text{ M } n\text{Bu}_4\text{NPF}_6/\text{CH}_2\text{Cl}_2, 17 \text{ }^\circ\text{C}) = 0.212 \pm 0.001 \text{ V}$ . The electro-active area of the Pt disc electrode was calculated from  $\text{Fc}/[\text{Fc}]^+$  measurements in 0.1 M  $n\text{Bu}_4\text{NPF}_6$  solution in  $\text{CH}_2\text{Cl}_2$  at various concentrations and potential sweep rates at 295 K, using  $D(\text{Fc}, \text{CH}_2\text{Cl}_2, 295 \text{ K}) = 2.2 \times 10^{-5} \text{ cm}^2 \text{ s}^{-1}$ .<sup>30</sup> The working electrode was rinsed with acetone, polished gently with a paste of 0.3  $\mu\text{m}$  alumina (Deutsche Metrohm GmbH & Co. KG) in deionized water, rinsed thoroughly with plenty of deionized water, and finally acetone after each use. Periodic  $\text{Fc}/[\text{Fc}]^+$  reference measurements verified the electro-active surface area of the Pt electrode, and the stability of the potential of the  $\text{Ag}/\text{Ag}^+$  reference electrode.

### 3 Synthetic Procedures and Analytical Data



$^{\text{Mes}}\text{Pt-PCy}_3$ . Ligand  $\text{Mes}_2^t\text{Bu}_2(\text{SH})_2$  (500 mg, 0.78 mmol) and benzyl potassium (203 mg, 1.56 mmol) were suspended in 8.6 g toluene at r.t. The reaction mixture was stirred at r.t. until all benzyl potassium was consumed and a clear yellow solution formed (30 min). The solvent was removed under vacuum and slightly yellow solid was obtained. *Trans*- $\text{py}_2\text{PtCl}_2$  (330 mg, 0.78 mmol) and  $\text{PCy}_3$  (218 mg, 0.78 mmol) were stirred in 31.89 g 1,2- $\text{C}_6\text{H}_4\text{F}_2$  until a white solid was formed (2 h). Ligand salt was diluted in 20 mL 1,2- $\text{C}_6\text{H}_4\text{F}_2$  and was added to the stirring precursor suspension. The flask was washed with 5 mL 1,2- $\text{C}_6\text{H}_4\text{F}_2$ . After addition of the ligand salt the solution turns reddish-orange. The reaction mixture was stirred for 3 d at r.t. The green solution was centrifuged, filtered of and the remaining KCl was washed three times with 3 mL 1,2- $\text{C}_6\text{H}_4\text{F}_2$ . The solvent was removed under vacuum and the dry green solid was diluted in 1,2- $\text{C}_6\text{H}_4\text{F}_2$ . The solution was concentrated until some crystals were formed and stored at 8 °C to obtain a crystalline  $^{\text{Mes}}\text{Pt-PCy}_3 \times 2(1,2\text{-C}_6\text{H}_4\text{F}_2)$  suitable for XRD analysis. The crystals were washed with pentane and dried under vacuum to afford 564 mg (58 %)  $^{\text{Mes}}\text{Pt-PCy}_3 \times 2(1,2\text{-C}_6\text{H}_4\text{F}_2)$ . Unit cell parameters:  $a = 9.8530(2)$  Å,  $b = 31.8471(6)$  Å,  $c = 20.0163(4)$  Å,  $\alpha = 90^\circ$ ,  $\beta = 93.0630(10)^\circ$ ,  $\gamma = 90^\circ$ ,  $V = 6271.93$  Å<sup>3</sup>,  $Z = 2$ ,  $I2/m$ , CCDC deposition number 1960797. Elemental analysis calcd for  $\text{C}_{69}\text{H}_{88}\text{F}_2\text{P}_2\text{PtS}_2$ : C, 66.53; H, 7.12; S, 5.15; F, 3.05. Found: C, 61.39; H, 7.67; S, 5.70. UV/vis/NIR ( $\text{CH}_2\text{Cl}_2$ , 20°C):  $\lambda(\epsilon) = 320$  (33.0), 350 (16.4), 580 nm ( $0.2 \times 10^3 \text{ mol}^{-1} \text{ dm}^3 \text{ cm}^{-1}$ ).  $^1\text{H}$  NMR (500 MHz,  $\text{CD}_2\text{Cl}_2$ , 25°C):  $\delta = 7.58$  (s, 4H; H8, H9, H11, H12), 7.27 (d,  $^4J_{\text{HH}} = 2.4$  Hz, 2H; H3, H18), 6.87 (d,  $^4J_{\text{HH}} = 2.4$  Hz, 2H; H5, H16), 6.85 (s, 4H; H23, H25, H29, H31), 2.24 (s, 6H; H40, H43), 2.00 (s, 12H; H39, H41, H42, H44), 1.47-1.39 (m, 15H;  $\text{PCy}_3$ ), 1.33 (s, 18H; H33-H38), 1.31-1.18 (m, 10H;  $\text{PCy}_3$ ), 1.06-0.97 (m, 3H;  $\text{PCy}_3$ ), 0.75 ppm (s, 5H;  $\text{PCy}_3$ ).  $^{13}\text{C}\{^1\text{H}\}$  NMR (125 MHz,  $\text{CD}_2\text{Cl}_2$ , 25°C):  $\delta = 145.8$  (C4, C17), 140.6 (C2, C13), 140.5 (C21, C27), 140.4 (C6, C15), 137.9 (C7, C10), 136.4 (C24, C30), 136.1 (C22, C26, C28, C32), 136 (d,  $^3J_{\text{CP}} = 2.8$  Hz; C1, C14), 128.2 (C23, C25, C29, C31), 127.8 (C5, C16), 122.3 (C3, C18), 34.4 (19, C20), 31.6 (C33-C38), 29.9 ( $\text{PCy}_3$ ), 26.9 ( $\text{PCy}_3$ ), 21.2 ppm (C40, C43).  $^{31}\text{P}$  NMR ( $\text{CD}_2\text{Cl}_2$ , 202 MHz):  $\delta = 31.68$  (d,  $^1J_{\text{PtP}} = 4398$  Hz).  $^{155}\text{Pt}$  NMR (129 MHz,  $\text{CD}_2\text{Cl}_2$ , 25°C):  $\delta = -4708$  (d,  $^1J_{\text{PtP}} = 4398$  Hz).

$^t\text{BuPt-PCy}_3$ . Ligand  $^t\text{Bu}_4(\text{SH})_2$  (500 mg, 0.96 mmol) and benzyl potassium (251 mg, 1.93 mmol) were suspended in 25 mL toluene at r.t., the reaction mixture was stirred until benzyl potassium was fully

consumed (30 min), and final solvent removal under vacuum afforded a pale yellow solid. *Trans*-py<sub>2</sub>PtCl<sub>2</sub> (409 mg, 0.96 mmol) and PCy<sub>3</sub> (270 mg, 0.96 mmol) were stirred in 16 mL 1,2-C<sub>6</sub>H<sub>4</sub>F<sub>2</sub> until a white solid formed (2 h) after which ligand potassium diluted in 20 mL of 1,2-C<sub>6</sub>H<sub>4</sub>F<sub>2</sub> was added, affording a reddish-orange solution. The reaction mixture was degassed by three freeze-pump-thaw cycles and stirred at 65 °C for 24 h during which the solution gradually turned dark green. The solvent was removed under vacuum, the residue dissolved in 1,2-C<sub>6</sub>H<sub>4</sub>F<sub>2</sub>, the green solution centrifuged to aid the filtration of KCl by that was washed three times with 3 mL of 1,2-C<sub>6</sub>H<sub>4</sub>F<sub>2</sub>. The solution was concentrated until crystals deposited and stored at 8 °C to afford crystalline material suitable for XRD analysis, and crystals were separated, washed with pentane, and finally dried under vacuum. Yield: 459 mg (47 %). Unit cell parameters:  $a = 9.8047(5) \text{ \AA}$ ,  $b = 11.4455(5) \text{ \AA}$ ,  $c = 21.2480(9) \text{ \AA}$ ,  $\alpha = 87.825(2)^\circ$ ,  $\beta = 85.279(2)^\circ$ ,  $\gamma = 81.634(2)^\circ$ ,  $V = 2350.25 \text{ \AA}^3$ ,  $Z = 2$ , P-1, CCDC deposition number 1960796. Elemental analysis calcd for C<sub>53</sub>H<sub>80</sub>PPtS<sub>2</sub>: C, 63.19; H, 8.00; S, 6.36. Found: C, 62.17; H, 7.57; S, 6.49. UV/vis/NIR (CH<sub>2</sub>Cl<sub>2</sub>, 20°C):  $\lambda(\epsilon)=289$  (29.7), 320 (30.5), 344 (19.0), 586 (0.2), 647 nm ( $0.2 \times 10^3 \text{ mol}^{-1} \text{ dm}^3 \text{ cm}^{-1}$ ). <sup>1</sup>H NMR (600 MHz, C<sub>6</sub>D<sub>6</sub>, 25°C):  $\delta=7.65$  (d, <sup>4</sup>J<sub>HH</sub>=2.4 Hz, 2H; H5, H16), 7.47 (d,  $J_{H,H}=1.4$  Hz, 4H; H8, H9, H10, H11), 7.28 (d, <sup>4</sup>J<sub>HH</sub>=2.4 Hz, 2H; H3, H18), 3.00 (m, 3H; PCy<sub>3</sub>), 1.95 (s, 18H; H29-H34), 1.91 (m, 6H; PCy<sub>3</sub>), 1.56 (m, 15H; PCy<sub>3</sub>), 1.36 (s, 18H; H23-H28), 1.19 (m, 6H; PCy<sub>3</sub>), 1.03 ppm (m, 3H; PCy<sub>3</sub>). <sup>13</sup>C{<sup>1</sup>H} NMR (150 MHz, C<sub>6</sub>D<sub>6</sub>, 25°C):  $\delta=147.6$  (C6, C15), 144.9 (C4, C17), 141.1 (C7, C10), 140.3 (C2, C13), 136.0 (d, <sup>3</sup>J<sub>CP</sub>=3.4 Hz; C1, C14), 124.6 (C5, C16), 122.5 (C3; C18), 116.8 (C8, C9, C11, C12), 38.3 (C21, C22), 34.5 (C19, C20), 32.2 (d,  $J_{CP}=32.5$  Hz; PCy<sub>3</sub>), 31.6 (C23-C28), 31.2 (C29-C34), 29.8 (PCy<sub>3</sub>), 27.6 (d,  $J_{CP}=11.4$  Hz; PCy<sub>3</sub>), 26.8 ppm (PCy<sub>3</sub>). <sup>31</sup>P NMR (242 MHz, C<sub>6</sub>D<sub>6</sub>, 25°C):  $\delta=37.01$  ppm (d, <sup>1</sup>J<sub>Pt</sub>=4638 Hz). <sup>135</sup>Pt NMR (129 MHz, C<sub>6</sub>D<sub>6</sub>, 25°C):  $\delta=-4638$  ppm (d, <sup>1</sup>J<sub>Pt</sub>=4638 Hz).

<sup>t</sup>BuPt-PPh<sub>3</sub>. Synthesis protocol as for <sup>t</sup>BuPt-PCy<sub>3</sub> using PPh<sub>3</sub> (253 mg, 0.96 mmol). Crystallisation from toluene afforded a greenish brown crystalline material. Yield: 333 mg (32 %) <sup>t</sup>BuPt-PPh<sub>3</sub>×C<sub>7</sub>H<sub>8</sub>. Crystals suitable for XRD analysis were obtained by diffusion of pentane into a toluene solution at r.t. Unit cell parameters:  $a = 11.4924(3) \text{ \AA}$ ,  $b = 13.2351(4) \text{ \AA}$ ,  $c = 15.9600(5) \text{ \AA}$ ,  $\alpha = 11.4924(3)^\circ$ ,  $\beta = 94.527(2)^\circ$ ,  $\gamma = 99.208(2)^\circ$ ,  $V = 2281.76 \text{ \AA}^3$ ,  $Z = 2$ , P-1, , CCDC deposition number 1960801. Elemental composition calcd for C<sub>53</sub>H<sub>62</sub>PPtS<sub>2</sub>: C, 64.35; H, 6.32; S, 6.48. Found: C, 64.10; H, 5.95; S, 6.58. UV/vis/NIR (CH<sub>2</sub>Cl<sub>2</sub>, 20°C):  $\lambda(\epsilon)=327$  (29.1), 360 (19.3), 424 (1.6), 561 nm ( $0.3 \times 10^3 \text{ mol}^{-1} \text{ dm}^3 \text{ cm}^{-1}$ ). <sup>1</sup>H NMR (500 MHz, CDCl<sub>3</sub>, 25°C):  $\delta=7.61-7.57$  (m, 5H; PPh<sub>3</sub>), 7.53 (s, 4H; H8, H9, H11, H12), 7.39-7.36 (m, 3H; PPh<sub>3</sub>), 7.34 (d, <sup>4</sup>J<sub>HH</sub>=2.3 Hz, 2H; H5, H16), 7.29-7.25 (m, 8H; PPh<sub>3</sub>), 7.22 (d, <sup>4</sup>J<sub>H,H</sub>=2.3 Hz, 2H; H3, H18), 1.33 (s, 18H; H23-H28), 1.10 ppm (s, 18H; H29-H34). <sup>13</sup>C{<sup>1</sup>H} NMR (125 MHz, CDCl<sub>3</sub>, 25°C):  $\delta=148.0$  (C6, C15), 145.1 (C4, C17), 140.6 (C7, C10), 140.2 (C2, C13), 135.5 (C1, C14), 135.4 (d,  $J_{CP}=10.8$  Hz; PPh<sub>3</sub>), 130.8 (PPh<sub>3</sub>), 127.8 (d,  $J_{CP}=11.5$  Hz; PPh<sub>3</sub>), 124.6 (C5, C16), 121.9 (C3, C18), 115.2 (C8, C9, C11, C12), 37.4 (C21, C22), 34.5 (C19, C20), 31.5

(H33-H38), 30.3 ppm (C29-C34).  $^{31}\text{P}$  NMR (202 MHz,  $\text{CDCl}_3$ , 25°C):  $\delta=32.70$  ppm (d,  $^1J_{\text{PPt}}=4868$  Hz)  $^{135}\text{Pt}$  NMR (129 MHz,  $\text{CDCl}_3$ , 25°C):  $\delta=-4674$  ppm (d,  $^1J_{\text{P,Pt}}=4868$  Hz).

$^{\text{Mes}}\text{Pd-PCy}_3$ . Ligand  $\text{Mes}_2^t\text{Bu}_2(\text{SH})_2$  (500 mg, 0.78 mmol) and benzyl potassium (203 mg, 1.56 mmol) were suspended in 17.5 g toluene at r.t. The reaction mixture was stirred at r.t. until all benzyl potassium was consumed and a clear yellow solution was formed. To this solution *trans*- $\text{py}_2\text{PdCl}_2$  suspended in 8.75 g toluene was added. The solution turns reddish-orange. Then  $\text{PCy}_3$  in 8.75 g toluene was added and the solution becomes brown. After stirring for 16 h at r.t. the reaction mixture was degassed by freeze-pump-thaw technique and then heated up to 60°C for 4 h. The brown solution was centrifuged, filtered off and the remaining KCl was washed three times with 3 mL toluene. The solvent was removed under vacuum and the brown-yellow solid was extracted with toluene. The solution was concentrated until some crystals were formed and pentane was added by slow diffusion at r.t. to obtain crystalline  $^{\text{Mes}}\text{Pd-PCy}_3 \times \text{C}_7\text{H}_8$  suitable for XRD analysis. The crystals were washed with pentane and dried under vacuum, losing half equivalent of toluene. Yield: 350 mg (40 %)  $^{\text{Mes}}\text{Pd-PCy}_3 \times 0.5(\text{C}_7\text{H}_8)$ . Unit cell parameters:  $a = 10.0757(3)$  Å,  $b = 16.5651(4)$  Å,  $c = 19.5789(6)$  Å,  $\alpha = 108.6390(10)^\circ$ ,  $\beta = 97.825(2)^\circ$ ,  $\gamma = 105.2480(10)^\circ$ ,  $V = 2899.46$  Å<sup>3</sup>,  $Z = 2$ , P-1, , CCDC deposition number 1960799. Elemental analysis calcd for  $\text{C}_{133}\text{H}_{176}\text{P}_2\text{Pd}_2\text{S}_4$ : C, 73.35; H, 8.15; S, 5.89. Found for two measurements of the same batch of crystalline material: C, 73.65/73.06; H, 7.44/8.00; S, 5.47/5.17. The high deviation could be caused by difficulties desorbing  $\text{H}_2\text{O}$  and  $\text{SO}_2$  properly separated from the device column. Therefore spectra  $^1\text{H}$ ,  $^{13}\text{C}\{^1\text{H}\}$  and  $^{31}\text{P}$  spectra of this batch are included in Figure S1 and S2. UV/vis/NIR ( $\text{CH}_2\text{Cl}_2$ , -80°C):  $\lambda(\epsilon)=315$  (17.0), 396 (33.5), 500 (0.4), 527 (0.3), 686 nm ( $0.2 \times 10^3 \text{ mol}^{-1} \text{ dm}^3 \text{ cm}^{-1}$ ).  $^1\text{H}$  NMR (600 MHz,  $\text{CD}_2\text{Cl}_2$ , 25°C):  $\delta=7.61$  (s, 4H; H8, H9, H11, H12), 7.31 (d,  $^4J_{\text{HH}}=2.3$  Hz, 2H; H3, H18), 6.86 (d,  $^4J_{\text{HH}}=2.3$  Hz, 2H; H5, H16), 6.85 (s, 4H; H23, H25, H29, H31), 2.56 (s, 3H;  $\text{PCy}_3$ ), 2.24 (s, 6H; H40, H43), 2.00 (s, 12H; H39, H41, H42, H44), 1.50-1.39 (m, 16H;  $\text{PCy}_3$ ), 1.34 (s, 18H; H33-H38), 1.25-1.16 (m, 6H;  $\text{PCy}_3$ ), 1.07-0.99 (m, 3H;  $\text{PCy}_3$ ), 0.86-0.70 ppm (m, 5H;  $\text{PCy}_3$ ).  $^{13}\text{C}\{^1\text{H}\}$  NMR (150 MHz,  $\text{CD}_2\text{Cl}_2$ , 25°C):  $\delta=145.9$  (C4, C17), 141.3 (C7, C10), 140.7 (C6, C15), 140.6 (C21, C27), 138.8 (C1, C14), 138.4 (C2, C13), 136.4 (C24, C30), 136.1 (C22, C26, C28, C32), 128.1 (C23, C25, C29, C31), 127.3 (C5, C16), 122.4 (C3, C18), 118.1 (C8, C9, C11, C12), 34.5 (C19, C20), 31.6 (C33-C38), 30.7 (d,  $J_{\text{PC}}=24.2$  Hz;  $\text{PCy}_3$ ), 30.4 ( $\text{PCy}_3$ ), 27.1 (d,  $J_{\text{PC}}=11.1$  Hz;  $\text{PCy}_3$ ), 26.8 ( $\text{PCy}_3$ ), 21.2 (C40, C43), 20.7 ppm (C39, C41, C42, C44).  $^{31}\text{P}$  NMR ( $\text{CD}_2\text{Cl}_2$ , 243 MHz):  $\delta=52.6$  ppm.

$^{\text{Mes}}\text{Pd-PPh}_3$ . Method 1:  $\text{Mes}_2^t\text{Bu}_2(\text{SH})_2$  (300 mg, 0.47 mmol), *trans*- $\text{py}_2\text{PdCl}_2$  (156 mg, 0.47 mmol) and  $\text{PPh}_3$  (122 mg, 0.47 mmol) were suspended in 23 mL toluene and  $\text{Et}_3\text{N}$  (0.15 mL, 0.98 mmol) was added. The yellow suspension turns red-orange after the addition of  $\text{Et}_3\text{N}$ . The reaction mixture was degassed by three freeze-pump-thaw cycles and heated to 55 °C for 2 h. The reaction mixture was then filtered off, and the residue washed three times with toluene. The brown solution was concentrated in vacuum and diffusion of pentane afforded brown needles, which were washed with pentane and dried

under vacuum. Yield: 286 mg (55 %) <sup>Mes</sup>Pd-PPh<sub>3</sub>×C<sub>7</sub>H<sub>8</sub>.

Method 2: Mes<sub>2</sub><sup>t</sup>Bu<sub>2</sub>(SH)<sub>2</sub> (300 mg, 0.47 mmol) and benzyl potassium (122 mg, 0.94 mmol) were suspended in 23 mL toluene. The reaction mixture was stirred at r.t. until all benzyl potassium was consumed (30 min). Then *trans*-py<sub>2</sub>PdCl<sub>2</sub> and PPh<sub>3</sub> were added and the reaction turns reddish. The mixture was degassed by freeze-pump-thaw-technique and heated for 10 h at 55 °C. The brown solution was centrifuged, filtered of and the residue was washed three times with toluene. The solution was concentrated in vacuum and by diffusion of pentane brown needles of the product with one equivalent toluene were obtained. The crystals were washed with pentane and dried under vacuum. Yield: 152 mg (30 %) <sup>Mes</sup>Pd-PPh<sub>3</sub>×C<sub>7</sub>H<sub>8</sub>.

Crystals suitable for XRD analysis were obtained by diffusion of pentane into a toluene solution at rt. Unit cell parameters:  $a = 9.4361(7)$  Å,  $b = 34.785(3)$  Å,  $c = 17.2103(12)$  Å,  $\alpha = 90^\circ$ ,  $\beta = 91.871(2)^\circ$ ,  $\gamma = 90^\circ$ ,  $V = 5646.01$  Å<sup>3</sup>,  $Z = 4$ , P21/n, CCDC deposition number 1960803. Elemental analysis calcd for C<sub>70</sub>H<sub>74</sub>PPdS<sub>2</sub>: C, 75.28; H, 6.68; S, 5.74. Found: C, 74.73; H, 6.22, S, 6.06. UV/vis/NIR (CH<sub>2</sub>Cl<sub>2</sub>, 20°C):  $\lambda(\epsilon)$ =409 (27.5), 528 (0.6), 681 nm ( $0.3 \times 10^3$  mol<sup>-1</sup>dm<sup>3</sup>cm<sup>-1</sup>). <sup>1</sup>H NMR (400 MHz, CD<sub>2</sub>Cl<sub>2</sub>, 25°C):  $\delta$ =7.67 (s, 4H; H8, H9, H11, H12), 7.37 (d, <sup>4</sup>J<sub>HH</sub>=2.3 Hz, 2H; H3, H18), 7.26-7.19 (m, 9H; PPh<sub>3</sub>), 7.12-7.07 (m, 6H; PPh<sub>3</sub>), 6.78 (d, <sup>4</sup>J<sub>HH</sub>=2.3 Hz, 2H; H5, H16), 6.61 (s, 4H; H23, H25, H29, H31), 2.24 (s, 6H; H40, H43), 1.66 (s, 12H; H39, H41, H42, H44), 1.32 (s, 4H; H33-H38). <sup>13</sup>C{<sup>1</sup>H} NMR (101 MHz, CD<sub>2</sub>Cl<sub>2</sub>, 25°C):  $\delta$ =146.1 (C4, C17), 141.1 (C7, C10), 140.8 (C6, C15), 139.6 (d, <sup>3</sup>J<sub>CP</sub>=9.9 Hz; C1, C14), 138.5 (C2, C13), 136.0 (C22, C26, C28, C32), 135.3 (C24, C30), 135.1 (d, <sup>3</sup>J<sub>CP</sub>=10.9 Hz; PPh<sub>3</sub>), 130.4 (PPh<sub>3</sub>), 127.7 (d, <sup>1</sup>J<sub>CP</sub>=11.2 Hz; PPh<sub>3</sub>), 127.7 (C23, C25, C29, C31), 127.2 (C5, C16), 122.3 (C3, C18), 117.9 (C8, C9, C11, C12), 34.5 (C19, C20), 31.5 (C33-C38), 21.1 (C40, C43), 20.3 ppm (C39, C41, C42, C44). <sup>31</sup>P NMR (162 MHz, CD<sub>2</sub>Cl<sub>2</sub>, 25°C):  $\delta$ =49.3 ppm. Diffusion coefficient  $D = 6.8 \times 10^{-10}$  m<sup>2</sup>/s (293 K, CD<sub>2</sub>Cl<sub>2</sub>).

[<sup>Mes</sup>Pt-PCy<sub>3</sub>]N(SO<sub>2</sub>CF<sub>3</sub>)<sub>2</sub>. To a solution of <sup>Mes</sup>Pt-PCy<sub>3</sub>×1,2-C<sub>6</sub>H<sub>4</sub>F<sub>2</sub> (92 mg, 0.074 mmol) in 4 mL of CH<sub>2</sub>Cl<sub>2</sub> was added [( $\eta^5$ -MeC(O)C<sub>5</sub>H<sub>4</sub>)<sub>2</sub>Fe]N(SO<sub>2</sub>CF<sub>3</sub>)<sub>2</sub> (41 mg, 0.074 mmol) in 2 mL of CH<sub>2</sub>Cl<sub>2</sub> at r.t. The dark purple solution was stirred for 2 min and was then cannula transferred into 100 mL of vigorously stirred pentane. A dark purple solid precipitated, and the reaction mixture was stored at -28°C overnight. An orange mother liquor was removed, and the purple solid recrystallized from CH<sub>2</sub>Cl<sub>2</sub> layered with pentane (1:10) at -28°C. The crystals thus obtained were washed with pentane three times and dried under vacuum. Yield: 77 mg (74 %). Crystals suitable for XRD analysis were obtained from diffusion of pentane into a 1,2-C<sub>6</sub>H<sub>4</sub>F<sub>2</sub> solution at -38°C. Unit cell parameters:  $a = 27.4740(10)$  Å,  $b = 29.3018(10)$  Å,  $c = 10.8540(4)$  Å,  $\alpha = \beta = \gamma = 90^\circ$ ,  $V = 8737.88$  Å<sup>3</sup>,  $Z = 8$ , Pnma, CCDC deposition number 1960802. Elemental analysis calcd for C<sub>65</sub>H<sub>84</sub>F<sub>6</sub>NO<sub>4</sub>PPtS<sub>4</sub>: C, 55.30; H, 6.00; N, 0.99; S, 9.08. Found: C, 54.93; H, 5.93; N, 0.99; S, 9.23.  $\mu_{\text{eff}} = 2.1$  (278–308 K, CD<sub>2</sub>Cl<sub>2</sub> containing 1,1,2,2-C<sub>2</sub>H<sub>2</sub>Cl<sub>4</sub>). UV/vis/NIR (CH<sub>2</sub>Cl<sub>2</sub>, 20°C):  $\lambda(\epsilon)$ =348 (15.9), 368 (17.4), 485 (2.7), 535 (2.6), 631 (1.1), 686 (0.4), 809 (0.9), 949 (0.3), 1526 nm ( $18.3 \times 10^3$  mol<sup>-1</sup>dm<sup>3</sup>cm<sup>-1</sup>).

$[\text{MesPt-PCy}_3]\text{BAR}^{\text{F}_4}$ .  $\text{MesPt-PCy}_3 \times 1,2\text{-C}_6\text{H}_4\text{F}_2$  (50 mg, 0.04 mmol) was dissolved in 1.5 mL of  $\text{CH}_2\text{Cl}_2$  and cooled to  $-78^\circ\text{C}$  in an aceton/dry ice bath, and combined with a solution of  $[(4\text{-BrC}_6\text{H}_4)_3\text{N}]\text{BAR}^{\text{F}_4}$  (54 mg, 0.04 mmol) in 0.5 mL of  $\text{CH}_2\text{Cl}_2$  that was transferred by cannula. The resulting dark purple solution was layered with pentane (1:10) and stored at  $-28^\circ\text{C}$ , affording dark purple crystals that were washed with pentane three times and dried under vacuum. Yield: 49 mg (61 %). Crystals suitable for XRD analysis were obtained by diffusion of pentane into a 1,1,2,2- $\text{C}_2\text{H}_2\text{Cl}_4$  solution at  $-38^\circ\text{C}$ . Unit cell parameters:  $a = 15.1784(6) \text{ \AA}$ ,  $b = 16.5068(6) \text{ \AA}$ ,  $c = 21.9412(8) \text{ \AA}$ ,  $\alpha = 84.293(2)^\circ$ ,  $\beta = 72.914(2)^\circ$ ,  $\gamma = 71.728(2)^\circ$ ,  $V = 4989.56 \text{ \AA}^3$ ,  $Z = 4$ , P-1, CCDC deposition number 1960800. Elemental analysis calcd for  $\text{C}_9\text{H}_9\text{BF}_4\text{PtS}_2$ : C, 57.20; H, 4.85; S, 3.21. Found: C, 57.04; H, 4.93; S, 3.18. UV/vis/NIR ( $\text{CH}_2\text{Cl}_2$ ,  $20^\circ\text{C}$ ):  $\lambda(\epsilon) = 349$  (19.4), 367 (20.9), 486 (2.9), 533 (2.8), 636 (1.0), 812 (0.5), 1530 nm ( $21.7 \times 10^3 \text{ mol}^{-1}\text{dm}^3\text{cm}^{-1}$ ). UV/vis/NIR (propylene carbonate,  $20^\circ\text{C}$ ):  $\lambda(\epsilon) = 269$  (40.8), 352 (15.1), 492 (1.7), 536 (1.8), 678 (0.7), 830 (0.8), 965 (0.7), 1511 nm ( $15.3 \times 10^3 \text{ mol}^{-1}\text{dm}^3\text{cm}^{-1}$ ).

$[\text{tBuPt-PCy}_3]\text{N}(\text{SO}_2\text{CF}_3)_2$ . Same procedure as for  $[\text{MesPt-PCy}_3]\text{N}(\text{SO}_2\text{CF}_3)_2$  starting from  $\text{tBuPt-PCy}_3$  (100 mg, 0.1 mmol) afforded a dark purple crystalline solid. Yield: 96 mg (75 %). Elemental analysis calcd for  $\text{C}_{55}\text{H}_{80}\text{F}_6\text{NO}_4\text{PtS}_4$ : C, 51.31; H, 6.26; N, 1.09; S, 9.96. Found: C, 50.48; H, 6.18; N, 1.16; S, 10.39;  $\mu_{\text{eff}} = 2.2$  (278–308 K,  $\text{CD}_2\text{Cl}_2$  containing 1,1,2,2- $\text{C}_2\text{H}_2\text{Cl}_4$ ). UV/vis/NIR ( $\text{CH}_2\text{Cl}_2$ ,  $20^\circ\text{C}$ ):  $\lambda(\epsilon) = 256$  (39.7), 278 (38.0), 347 (19.1), 377 (13.2), 502 (4.0), 554 (3.8), 657 (1.8), 746 (1.1), 926 (0.9), 1682 nm ( $15.4 \times 10^3 \text{ mol}^{-1}\text{dm}^3\text{cm}^{-1}$ ).

$[\text{tBuPt-PPh}_3]\text{N}(\text{SO}_2\text{CF}_3)_2$ . Same procedure as for  $[\text{MesPt-PCy}_3]\text{N}(\text{SO}_2\text{CF}_3)_2$  starting from  $\text{tBuPt-PPh}_3 \times \text{C}_7\text{H}_8$  (100 mg, 0.09 mmol) afforded a dark purple crystalline solid. Yield: 41 mg (35 %). Elemental analysis calcd for  $\text{C}_{55}\text{H}_{62}\text{F}_6\text{NO}_4\text{PtS}_4$ : C, 52.04; H, 4.92; N, 1.10; S, 10.10. Found: C, 51.61; H, 4.85; N, 1.22; S, 10.26.  $\mu_{\text{eff}} = 1.9$  (223–273 K,  $\text{CD}_2\text{Cl}_2$  containing 1,1,2,2- $\text{C}_2\text{H}_2\text{Cl}_4$ ). UV/vis/NIR ( $\text{CH}_2\text{Cl}_2$ ,  $-50^\circ\text{C}$ ):  $\lambda(\epsilon) = 374$  (6.3), 506 (3.1), 536 (3.0), 617 (1.2), 746 (0.3), 959 (0.7), 1539 nm ( $17.1 \times 10^3 \text{ mol}^{-1}\text{dm}^3\text{cm}^{-1}$ ).

$[\text{tBuPt-PPh}_3]\text{BAR}^{\text{F}_4}$ . Same procedure as for  $[\text{MesPt-PCy}_3]\text{BAR}^{\text{F}_4}$  starting from  $\text{tBuPt-PPh}_3 \times \text{C}_7\text{H}_8$  (50 mg, 0.046 mmol) afforded brown crystalline material. Yield: 41 mg (48 %). Dark brown single crystals suitable for XRD analysis separated at  $-38^\circ\text{C}$  from a  $\text{CH}_2\text{Cl}_2$  solution of  $[\text{tBuPt-PCy}_3]\text{BAR}^{\text{F}_4}$  layered with pentane. Unit cell parameters:  $a = 14.4458(3) \text{ \AA}$ ,  $b = 18.4681(4) \text{ \AA}$ ,  $c = 19.6025(4) \text{ \AA}$ ,  $\alpha = 107.0010(10)^\circ$ ,  $\beta = 108.6950(10)^\circ$ ,  $\gamma = 100.0160(10)^\circ$ , P-1, CCDC deposition number 1960798. Elemental analysis calcd for  $\text{C}_8\text{H}_7\text{BF}_4\text{PtS}_2$ : C, 55.11; H, 4.03; S, 3.46. Found: C, 54.74; H, 3.91; S, 3.86.

$[\text{MesPd-PCy}_3]\text{BAR}^{\text{F}_4}$ . Procedure as for  $[\text{MesPt-PCy}_3]\text{BAR}^{\text{F}_4}$  starting from  $\text{MesPd-PCy}_3 \times 0.5(\text{C}_7\text{H}_8)$  (50 mg, 0.046 mmol) afforded a dark red crystalline material. Yield: 59 mg (68%). Dark reddish brown crystals suitable for XRD analysis separated at  $-28^\circ\text{C}$  from a  $\text{CH}_2\text{Cl}_2$  solution layered with pentane. Unit cell parameters:  $a = 15.9777(3) \text{ \AA}$ ,  $b = 17.5645(3) \text{ \AA}$ ,  $c = 19.4418(3) \text{ \AA}$ ,  $\alpha = 111.6280(10)^\circ$ ,  $\beta =$

102.1630(10)°,  $\gamma = 92.6780(10)^\circ$ ,  $V = 4525.78 \text{ \AA}^3$ ,  $Z = 2$ , P-1, CCDC deposition number 1960804. Elemental analysis calcd for  $C_9H_9BF_2PPdS_2$ : C, 59.86; H, 5.08; S, 3.36. Found: C, 59.24; H, 5.13; S, 3.30. UV/vis/NIR ( $CH_2Cl_2$ , 20°C):  $\lambda(\epsilon)=277$  (51.1), 302 (27.8), 412 (14.5), 442 (14.4), 544 (5.6), 852 (1.7), 2210 nm ( $13.7 \times 10^3 \text{ mol}^{-1} \text{ dm}^3 \text{ cm}^{-1}$ ). UV/vis/NIR (propylene carbonate, -40°C):  $\lambda(\epsilon)=402$  (12.8), 432 (10.3), 538 (2.9), 862 (0.7), 2210 nm ( $6.2 \times 10^3 \text{ mol}^{-1} \text{ dm}^3 \text{ cm}^{-1}$ ).

#### 4 Additional Solid-State Structure Data

**Table S1** Selected bond lengths [ $\text{\AA}$ ] and angles [ $^\circ$ ] of neutral complexes.

	$\text{MesNi-PCy}_3^{\text{a}}$	$\text{MesPd-PCy}_3$	$\text{MesPt-PCy}_3$	$\text{tBuPt-PCy}_3$	$\text{tBuPt-PPh}_3$	$\text{MesPd-PPh}_3$
M-P	2.353(2)	2.3119(6)	2.2955(4)	2.2685(6)	2.2356(8)	2.263(1)
M-S1	2.222(2)	2.3729(5)	2.3719(3)	2.3827(6)	2.3433(7)	2.348(4)
S1-Ar	1.776(4)	1.778(2)	1.773(1)	1.791(2)	1.790(3)	1.782(3)
M-S2	2.259(2)	2.3725(6)	2.3719(3)	2.3604(6)	2.3809(6)	2.361(1)
S2-Ar	1.780(4)	1.769(2)	1.773(1)	1.792(2)	1.785(3)	1.774(3)
M-Ar <sup>b</sup>	2.179	2.305	2.273	2.271	2.254	2.313
P-M-Ar <sup>b</sup>	171.86	173.47	177.89	167.51	171.26	161.33
M-S1-CC	4.1(4)	2.3(2)	3.5	11.3(2)	19.8(3)	12.6(3)
M-S2-CC	13.3(4)	3.8(2)	3.5	15.1(2)	20.5(2)	9.5(3)

a) Data included for the sake of better comparability and taken from ref. <sup>13</sup>. b) Data determined using centroid of  $\eta^2$ -coordinate moiety of 1,4-disubstituted arene.

**Table S2** Selected bond lengths [Å] and angles [°] of radical cation complexes.

	[ <sup>Mes</sup> Pd-PCy <sub>3</sub> ]	[ <sup>Mes</sup> Pt-PCy <sub>3</sub> ]	[ <sup>Mes</sup> Pt-PCy <sub>3</sub> ]	[ <sup>Mes</sup> Pt-PPh <sub>3</sub> ]	[ <sup>tBu</sup> Pt-PPh <sub>3</sub> ]
	BAr <sup>F</sup> <sub>4</sub>	BAr <sup>F</sup> <sub>4</sub>	N(SO <sub>2</sub> CF <sub>3</sub> ) <sub>2</sub> <sup>a)</sup>	N(SO <sub>2</sub> CF <sub>3</sub> ) <sub>2</sub> <sup>b)</sup>	BAr <sup>F</sup> <sub>4</sub>
M-P	2.3155(7)	2.307(1)	2.320	2.2694(7)	2.2441(7)
M-S1	2.3238(7)	2.306(1)	2.296	2.3012(9)	2.3391(6)
S1-Ar	1.772(3)	1.761(4)	1.755(5)	1.760(2)	1.786(3)
M-S2	2.3276(7)	2.314(1)	2.296	2.3149(9)	2.3410(6)
S2-Ar	1.743(3)	1.758(6)	1.755(5)	1.760(2)	1.796(3)
M-Ar	2.366	2.356	2.313	2.270	2.296
P-M-Ar	164.70	170.33	172.26	174.62	169.81
M-S1-CC	8.8(3)	8.5(5)	4.2	18.8(2)	20.3(2)
M-S2-CC	4.9(3)	4.6(5)	4.2	3.2(2)	17.4(2)

a) The Pt atom locates at an inversion centre so metrical data are likely biased by symmetry of the crystal lattice. b) Data included for comparison and taken from ref. 16.

## 5 Additional NMR Spectroscopic Data

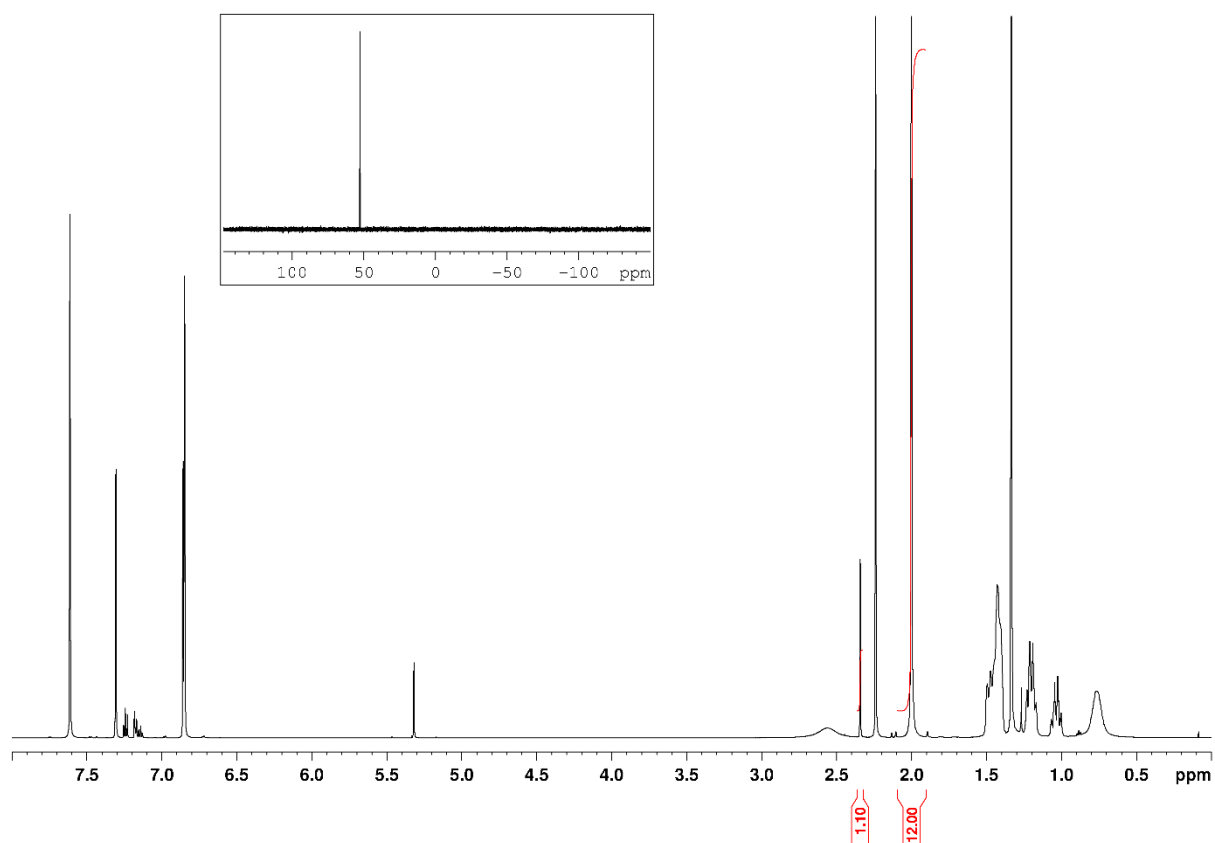


**Fig. S2**  $^1\text{H}$  NMR (600 MHz,  $\text{CD}_2\text{Cl}_2$ , 26°C) and  $^{31}\text{P}\{^1\text{H}\}$  NMR data (243 MHz  $\text{CD}_2\text{Cl}_2$ , 26°C; inset):  $\text{MesPd-PCy}_3 \times 0.5(\text{C}_7\text{H}_8)$ .

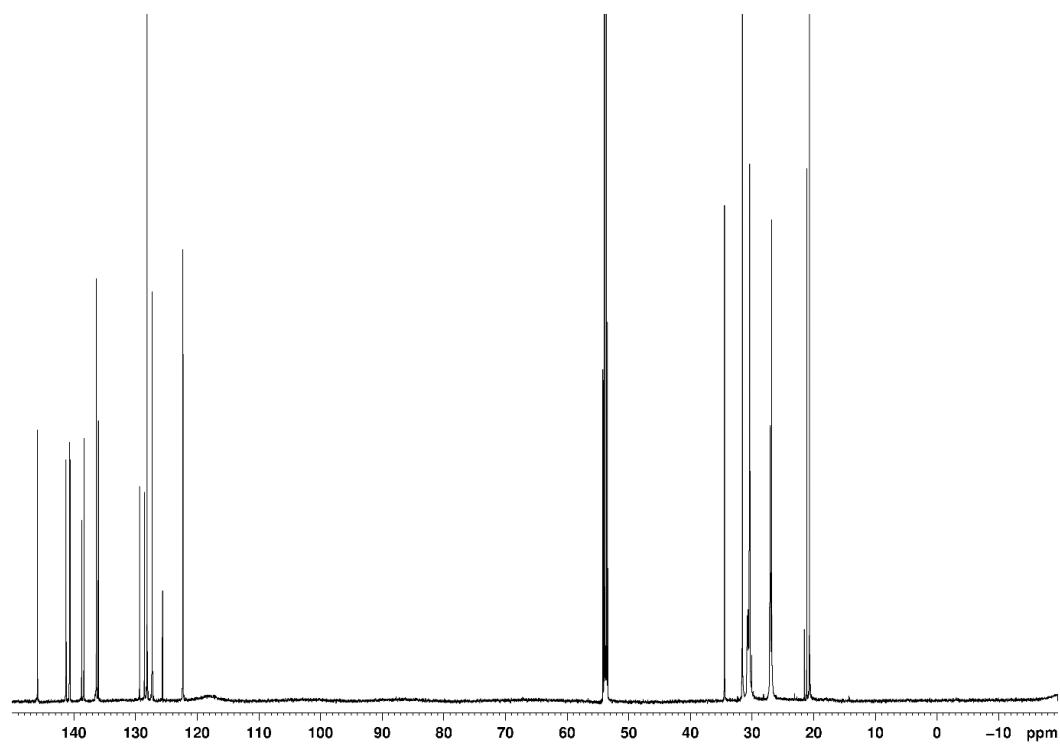


**Fig. S3**  $^{13}\text{C}\{^1\text{H}\}$  NMR (150 MHz,  $\text{CD}_2\text{Cl}_2$ , 26°C):  $\text{MesPd-PCy}_3 \times 0.5(\text{C}_7\text{H}_8)$ .

## 6 Additional Information on UV/Vis/NIR Spectroscopy Data

For *in situ* generation of  $[\text{MesM-L}]^+$  stock solutions of the neutral compound and the oxidizing agent in  $\text{CH}_2\text{Cl}_2$  at r.t. were prepared. A four-sided transparent cell with a screw cap and septum was filled with 2.8 mL  $\text{CH}_2\text{Cl}_2$ , and background spectra were recorded at  $-90 \leq T \leq 20$  °C at 10 °C steps. The neutral compound is then transferred by syringe to the cuvette at  $T \leq -80$  °C and a spectrum is recorded. Aliquots of 0.25 equiv., in the case of  $[\text{MesNi-PCy}_3]^+$  one equiv., of oxidizing agent are added, and spectra were recorded after each addition. The obtained spectra were corrected by subtraction of the respective background of neat  $\text{CH}_2\text{Cl}_2$ .

Due to insolubility at high concentrations the stock solution of  $[\text{MesPd-PCy}_3]\text{BAr}^{\text{F}_4}$  for measurements in PC were prepared in  $\text{CH}_2\text{Cl}_2$ . 2.8 mL of PC are added to a four-sided transparent cell with a screw cap and septum, and background spectra were recorded at  $-40 \leq T \leq 20$  °C. 15  $\mu\text{L}$  of the stock solution is added four times and a spectrum is recorded after each addition.

**Table S3** NIR data of  $[\text{R}^{\text{M-L}}]\text{X}$  ( $\text{X} = (\text{F}_3\text{CSO}_2)_2\text{N}^- (= \text{NTf}_2)$  and  $\text{Ar}^{\text{F}_4}\text{B}^-$ ) in  $\text{CH}_2\text{Cl}_2$  solution.

	$\lambda/$ nm	$\nu/$ $\text{cm}^{-1}$	$\Delta\nu_{1/2}/$ $\text{cm}^{-1}$	$\epsilon/ 10^4$ $\text{L mol}^{-1} \text{cm}^{-1}$	$T/$ K
$[\text{MesNi-PCy}_3]\text{NTf}_2$	2149	4653	1455	0.53	183
$[\text{MesNi-PCy}_3]\text{BAr}^{\text{F}_4}$	2157	4636	1454	0.43	183
$[\text{MesPd-PCy}_3]\text{NTf}_2$	2216	4512 (4502)	1108 (1241)	1.5	193 (293)
$[\text{MesPd-PCy}_3]\text{BAr}^{\text{F}_4}$	2210	4531 (4524)	1093 (1311)	1.5	183 (293)
$[\text{MesPd-PPh}_3]\text{NTf}_2$	2179	4589 (4596)	1100 (1260)	1.4	183 (293)
$[\text{MesPt-PCy}_3]\text{NTf}_2$	1526	6531 (6561)	1410 (1588)	1.8	193 (293)
$[\text{MesPt-PCy}_3]\text{BAr}^{\text{F}_4}$	1530	6540 (6535)	1394 (1672)	2.2	183 (293)
$[\text{tBuPt-PCy}_3]\text{NTf}_2$	1682	6090 (5945)	2056 (1944)	1.5	183 (293)
$[\text{tBuPt-PPh}_3]\text{NTf}_2$	1539	6497 (6406)	1544 (1698)	1.7	223 (293)

<sup>Mes</sup>Ni-PCy<sub>3</sub>. UV/vis/NIR (CH<sub>2</sub>Cl<sub>2</sub>, -90°C): λ(ε)=331 (20.4), 448 (3.2), 558 (6.9), 658 (3.0), 1058 nm (1.3×10<sup>3</sup> mol<sup>-1</sup>dm<sup>3</sup>cm<sup>-1</sup>).

[<sup>Mes</sup>Ni-PCy<sub>3</sub>]BAR<sup>F</sup><sub>4</sub>. UV/vis/NIR (CH<sub>2</sub>Cl<sub>2</sub>, -90°C): λ(ε)=436 (5.1), 564 (6.3), 657 (3.0), 1089 (3.1), 1297 (2.0), 2157 (3.7×10<sup>3</sup> mol<sup>-1</sup>dm<sup>3</sup>cm<sup>-1</sup>).

[<sup>Mes</sup>Ni-PCy<sub>3</sub>]N(SO<sub>2</sub>CF<sub>3</sub>)<sub>2</sub>. UV/vis/NIR (CH<sub>2</sub>Cl<sub>2</sub>, -90°C): λ(ε)=332 (20.2), 434 (6.8), 500 (6.1), 568 (6.7), 685 (3.3), 1098 (4.2), 1297 (2.9), 2149 (5.4×10<sup>3</sup> mol<sup>-1</sup>dm<sup>3</sup>cm<sup>-1</sup>).

[<sup>Mes</sup>Pd-PCy<sub>3</sub>]N(SO<sub>2</sub>CF<sub>3</sub>)<sub>2</sub>. UV/vis/NIR (CH<sub>2</sub>Cl<sub>2</sub>, -80°C): λ(ε)=436 (27.0), 538 (7.2), 797 (1.2), 863 (1.8), 1131 (0.5), 2216 (20×10<sup>3</sup> mol<sup>-1</sup>dm<sup>3</sup>cm<sup>-1</sup>).

[<sup>Mes</sup>Pd-PPh<sub>3</sub>]N(SO<sub>2</sub>CF<sub>3</sub>)<sub>2</sub>. UV/vis/NIR (CH<sub>2</sub>Cl<sub>2</sub>, -90°C): λ(ε)=407 (21.6), 534 (6.1), 832 (1.2), 1174 (0.8), 2179 (14×10<sup>3</sup> mol<sup>-1</sup>dm<sup>3</sup>cm<sup>-1</sup>). Diffusion coefficient *D* of Dimer = 4.8×10<sup>-10</sup> m<sup>2</sup>/ s (293 K, CD<sub>2</sub>Cl<sub>2</sub>).

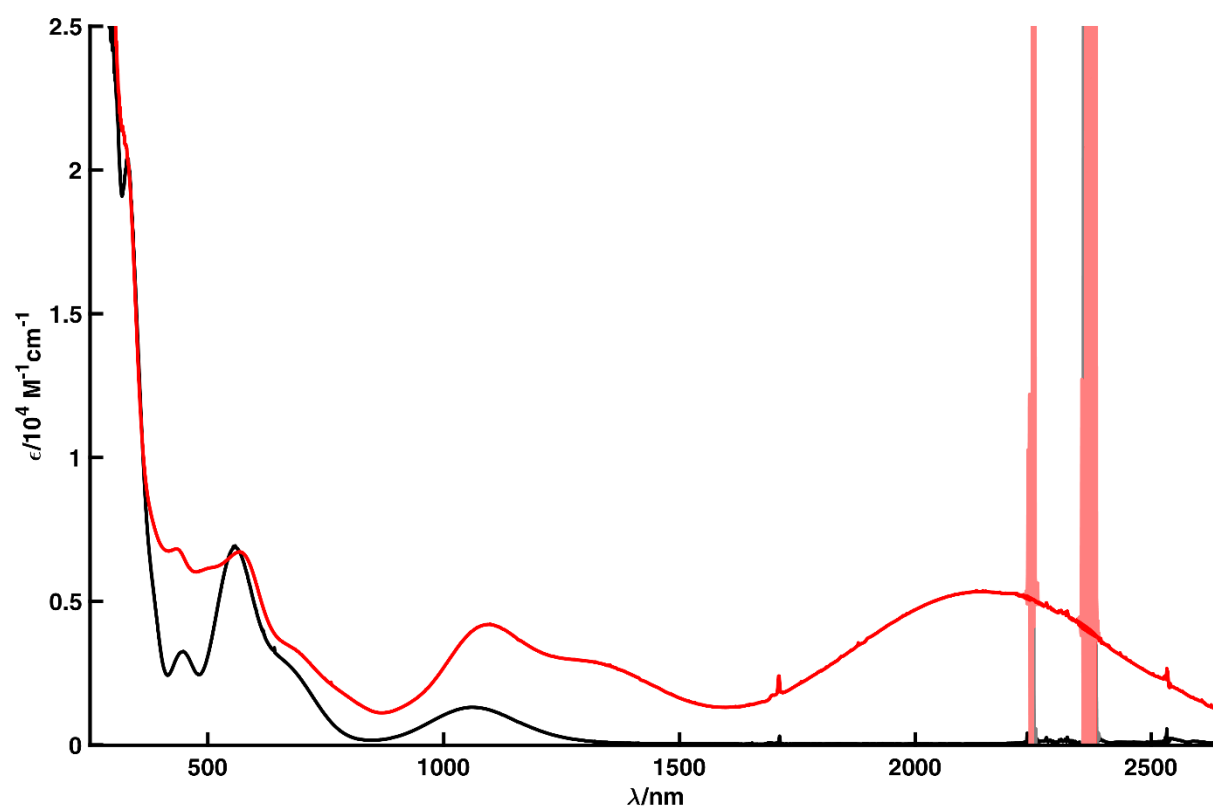


**Fig. S4** UV/vis/NIR spectra (CH<sub>2</sub>Cl<sub>2</sub>, -90°C): 0.144 mM [<sup>Mes</sup>Ni-PCy<sub>3</sub>]N(SO<sub>2</sub>CF<sub>3</sub>)<sub>2</sub> (red) and 0.151 mM <sup>Mes</sup>Ni-PCy<sub>3</sub> (black).

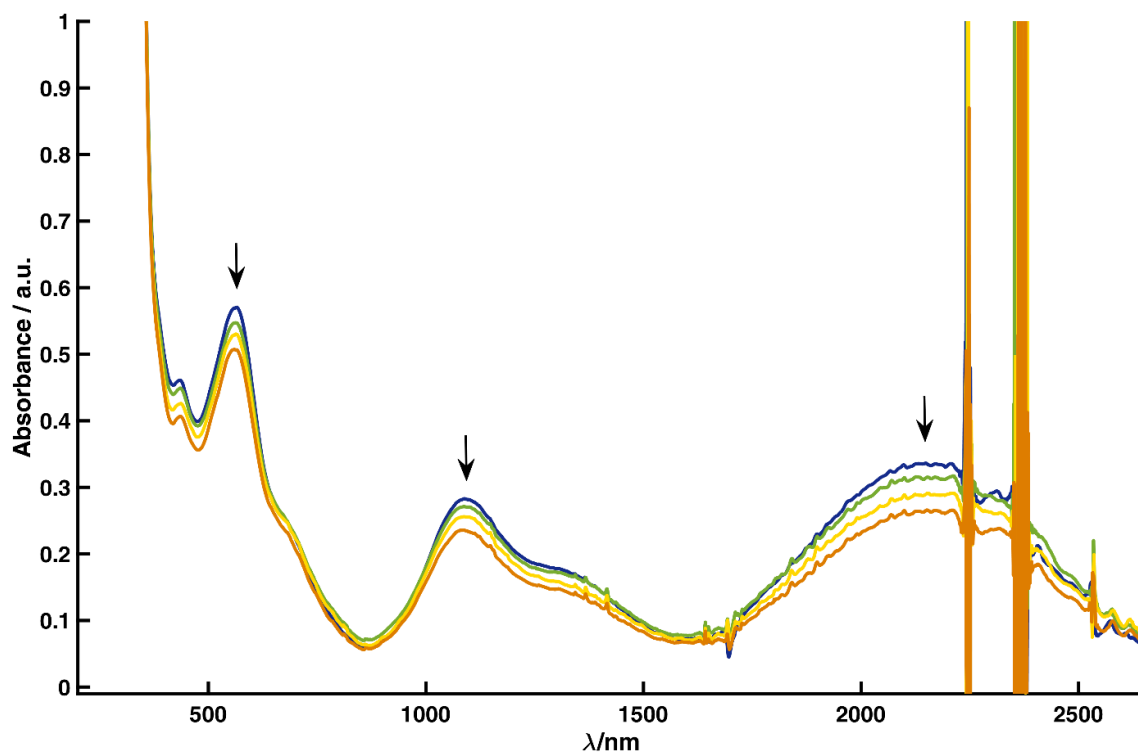


**Fig. S5** UV/vis/NIR spectra ( $\text{CH}_2\text{Cl}_2$ ,  $-90^\circ\text{C}$ ):  $0.087 \text{ mM } [\text{MesNi-PCy}_3]\text{BARF}_4$ , evolution of spectra monitored over 2 h.

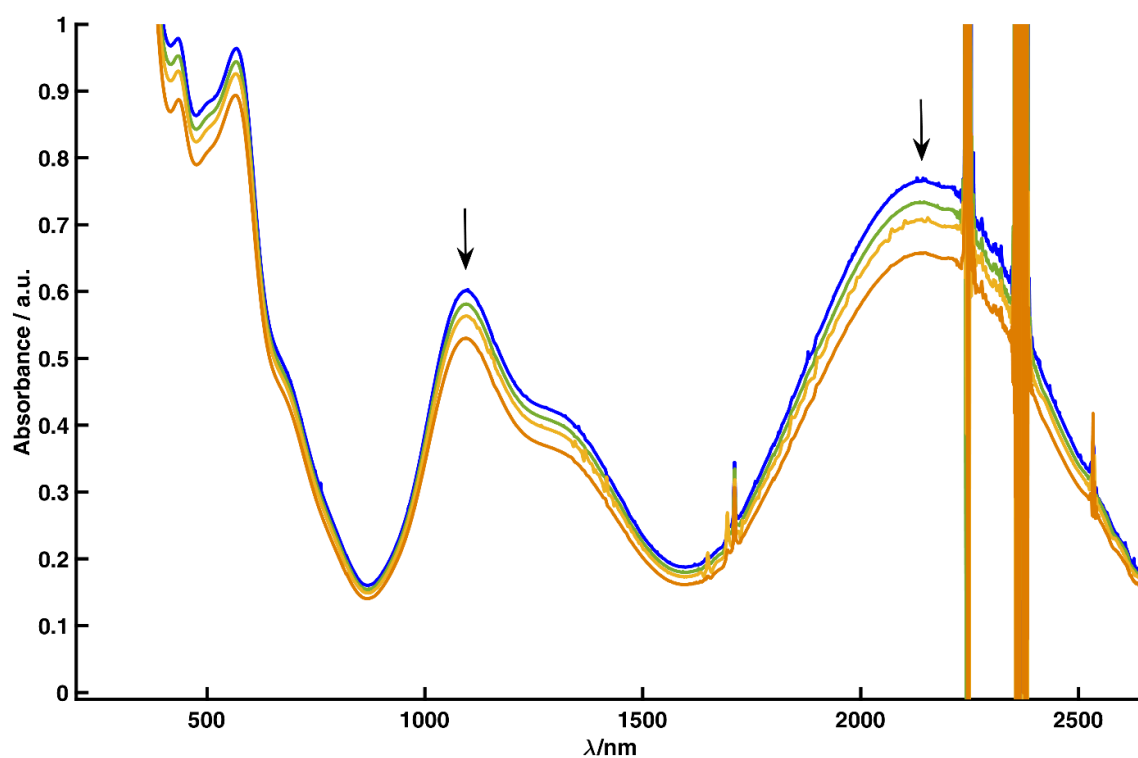


**Fig. S6** UV/vis/NIR spectra ( $\text{CH}_2\text{Cl}_2$ ,  $-90^\circ\text{C}$ ):  $0.144 \text{ mM } [\text{MesNi-PCy}_3]\text{N}(\text{SO}_2\text{CF}_3)_2$ , evolution of spectra monitored over 40 min.

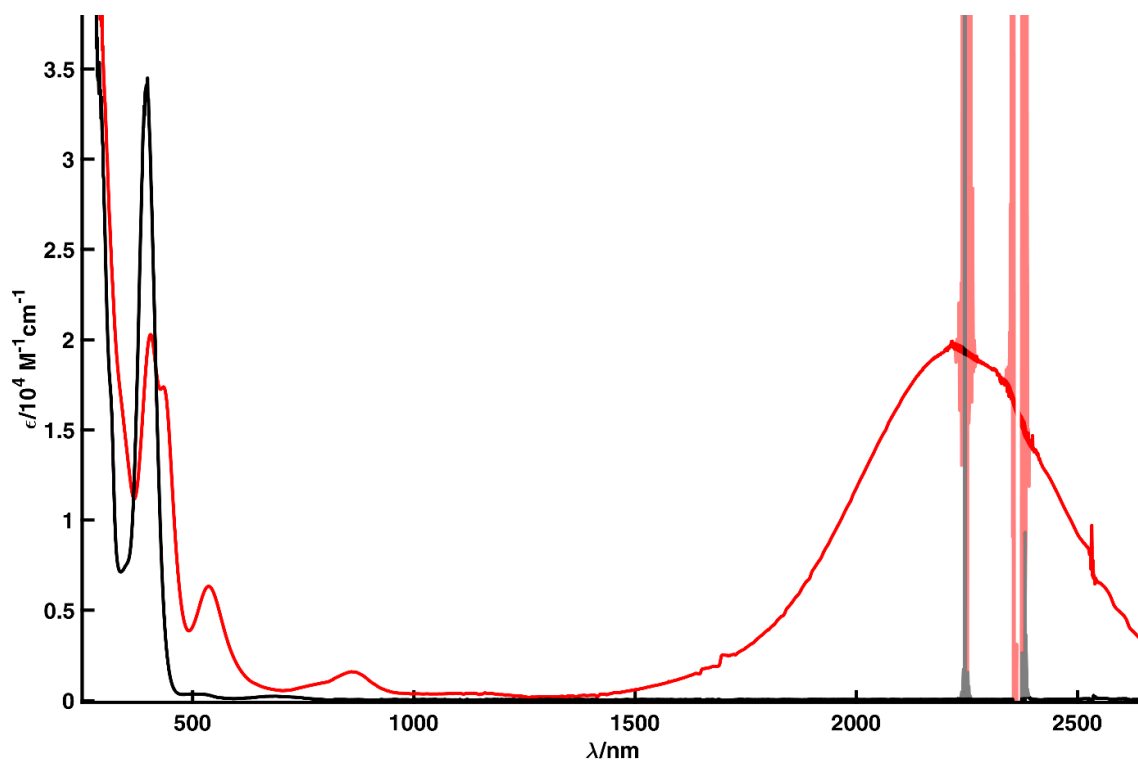


**Fig. S7** UV/vis/NIR spectra ( $\text{CH}_2\text{Cl}_2$ ,  $-80^\circ\text{C}$ ): 0.103 mM  $[\text{MesPd-PCy}_3]\text{N}(\text{SO}_2\text{CF}_3)_2$  (red) and 0.111 mM  $\text{MesPd-PCy}_3$  (black).

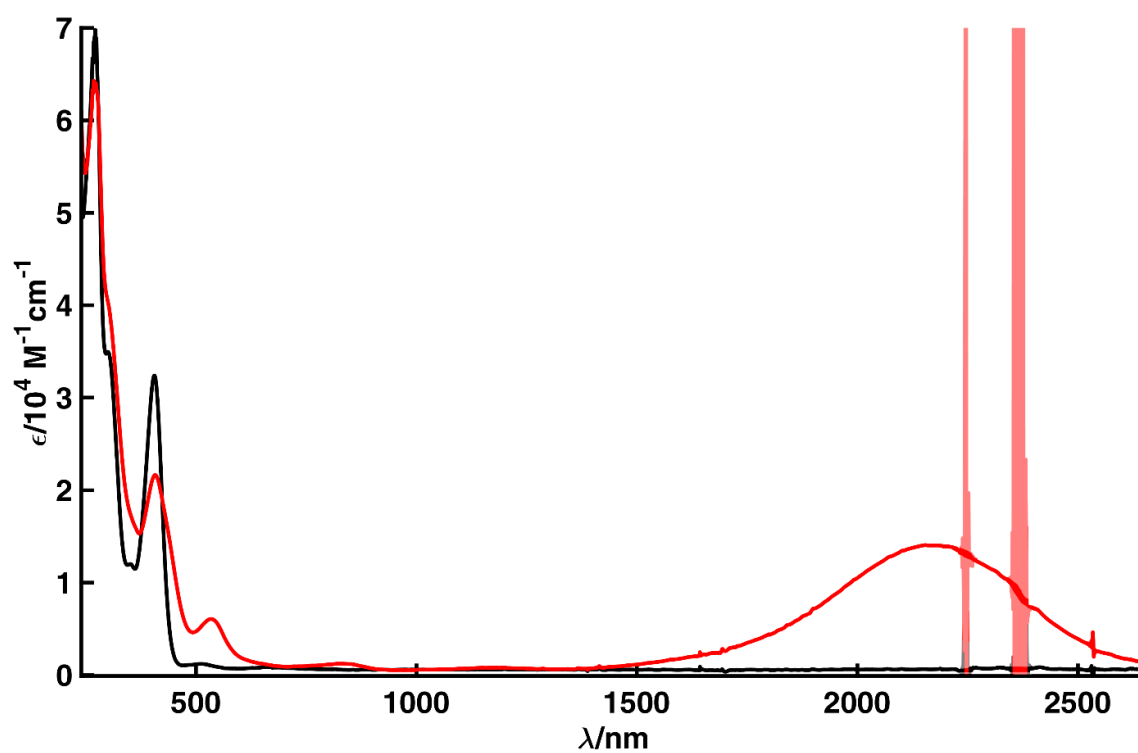


**Fig. S8** UV/vis/NIR spectra ( $\text{CH}_2\text{Cl}_2$ ,  $-90^\circ\text{C}$ ): 0.055 mM  $[\text{MesPd-PPh}_3]\text{N}(\text{SO}_2\text{CF}_3)_2$  (red) and 0.054 mM  $\text{MesPd-PPh}_3$  (black).

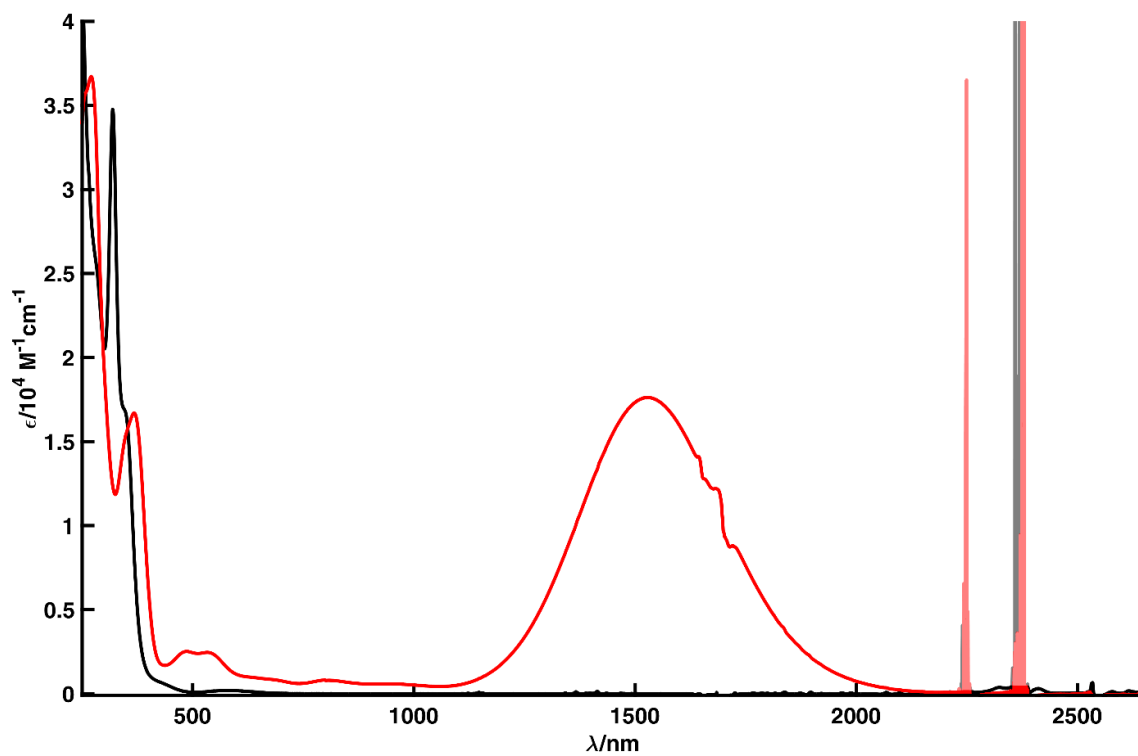


**Fig. S9** UV/vis/NIR spectra ( $\text{CH}_2\text{Cl}_2$ ,  $20^\circ\text{C}$ ):  $0.057 \text{ mM}$   $[\text{MesPt-PCy}_3]\text{N(SO}_2\text{CF}_3)_2$  (red) and  $0.052 \text{ mM}$   $^{\text{Mes}}\text{Pt-PCy}_3$  (black).

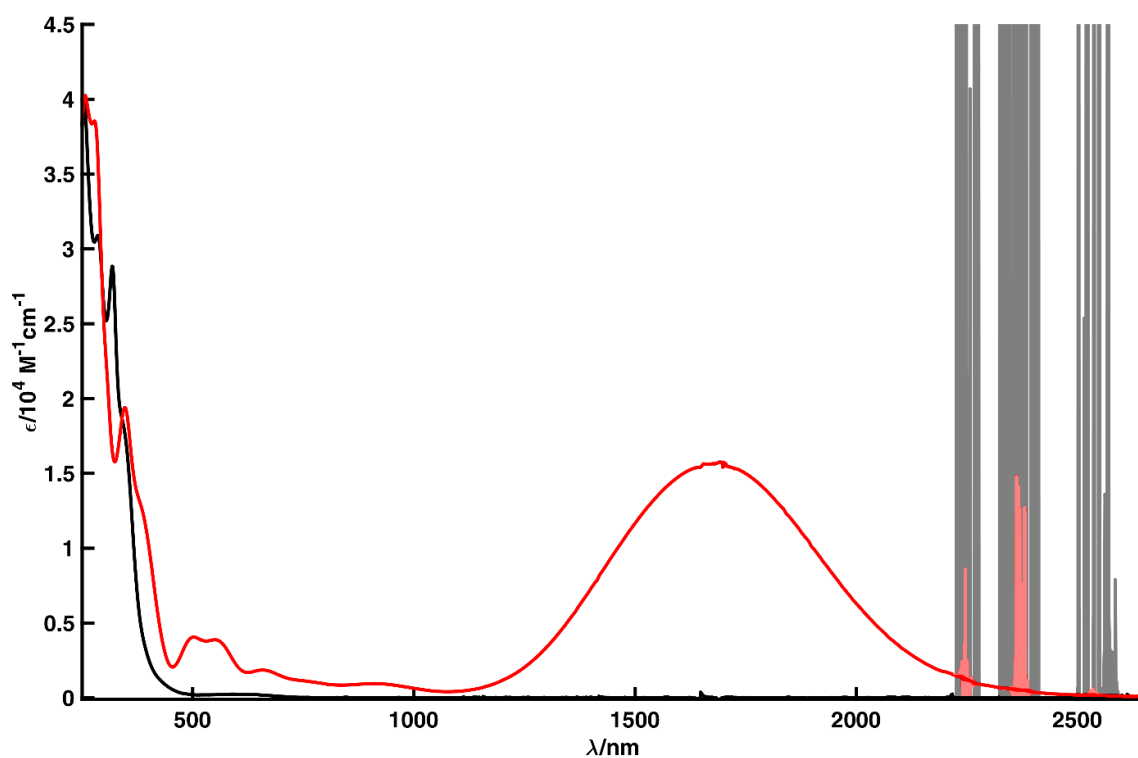


**Fig. S10** VT UV/vis/NIR spectra ( $\text{CH}_2\text{Cl}_2$ ,  $20^\circ\text{C}$ ):  $0.037 \text{ mM}$   $[\text{tBuPt-PCy}_3]\text{N(SO}_2\text{CF}_3)_2$  and  $0.063 \text{ mM}$   $^{\text{tBu}}\text{Pt-PCy}_3$  (black).

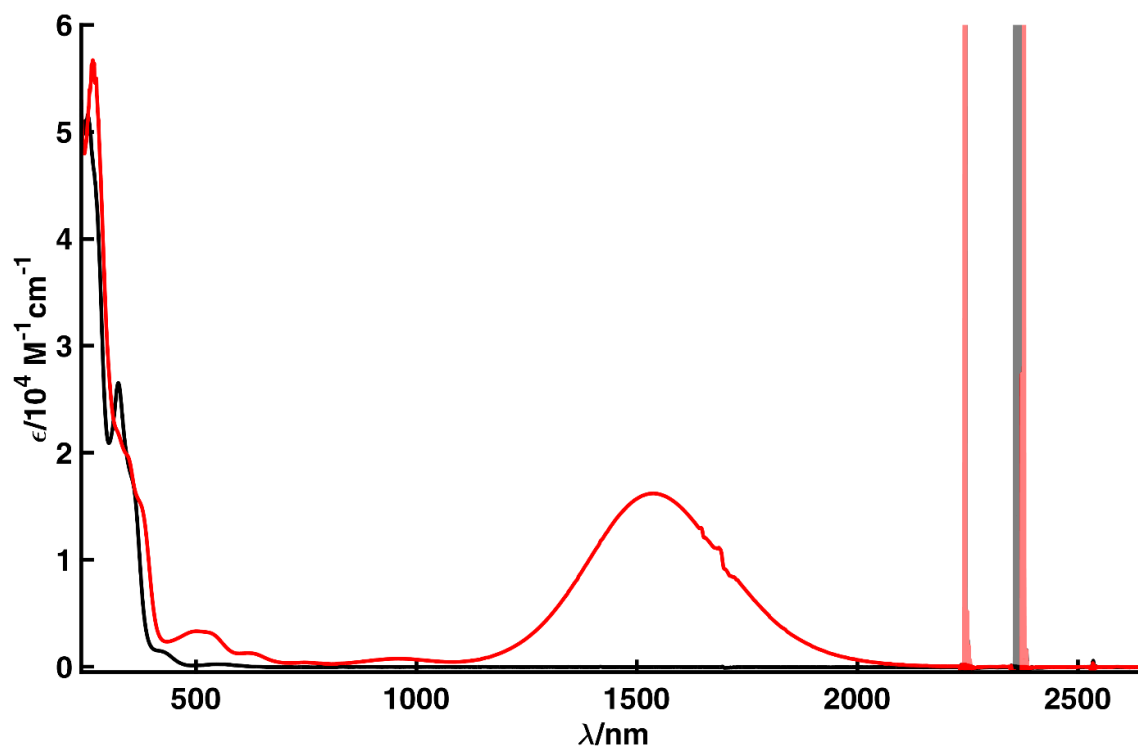
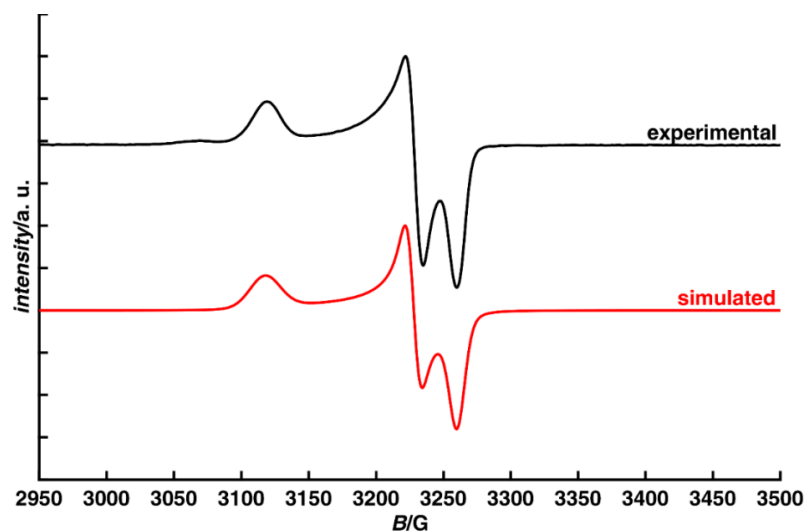


Fig. S11 UV/vis/NIR spectra ( $\text{CH}_2\text{Cl}_2$ ,  $-50^\circ\text{C}$ ):  $0.064 \text{ mM } [{}^{\text{iBu}}\text{Pt-PPh}_3]\text{N}(\text{SO}_2\text{CF}_3)_2$  and  $0.065 \text{ mM } {}^{\text{iBu}}\text{Pt-PPh}_3$  (black).

## 7 Additional X-Band cw-EPR Data

For the general *in situ* preparation, 4 mM stock solutions of the neutral complexes in toluene and of the oxidizing agent in  $\text{CH}_2\text{Cl}_2$  were prepared at r.t. For delicate samples, 0.25 mL of the neutral compound were transferred by syringe into an NMR tube sealed with a septum and cooled in an acetone/dry ice bath at  $-80\text{ }^\circ\text{C}$ . To this solution, 0.25 mL of the stock solution of the oxidizing agent were added slowly. The reactant solutions were mixed agitating the tube carefully, and finally frozen in liquid  $\text{N}_2$ .



**Fig. S12** X-Band cw-EPR spectra (1:1  $\text{C}_7\text{H}_8/\text{CH}_2\text{Cl}_2$ , 110 K):  $[\text{MesNi-PCy}_3]\text{N}(\text{SO}_2\text{CF}_3)_2$ , microwave frequency = 9.296928 GHz, microwave power = 0.7962 mW, modulation amplitude = 0.2 mT, Simulated parameters:  $g_x = 2.131$ ,  $g_y = 2.058$ ,  $g_z = 2.038$ ; full line width at half maximum (Gaussian; Lorentzian)  $lw = [0.929; 0.437]$  mT,  $g\text{Strain} = [0.0155; 0; 0.00410]$ .

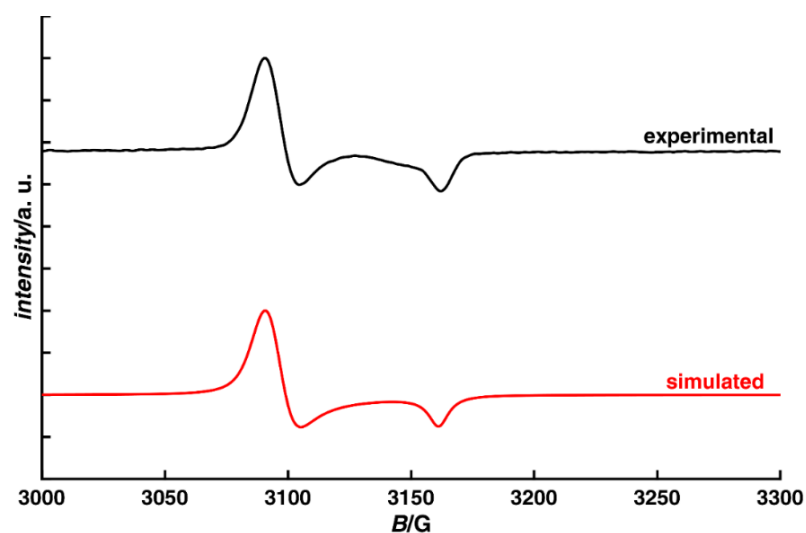


**Fig. S13** X-Band cw-EPR spectra (1:1  $\text{C}_7\text{H}_8/\text{CH}_2\text{Cl}_2$ , 110 K): Sample of  $[\text{MesNi-PCy}_3]\text{BARF}_4$  after keeping at r.t. for  $<5$  min. (initial spectrum identical with Fig. S12), microwave frequency = 9.256458 GHz, microwave power = 0.5024 mW, modulation amplitude = 0.2 mT, Simulated parameters:  $g_{x,y} = 2.138$ ,  $g_z = 2.092$ ; full line width at half maximum (Gaussian; Lorentzian)  $lw = [0.127; 0.946]$  mT,  $g\text{Strain} = [0.00696; 0]$ .

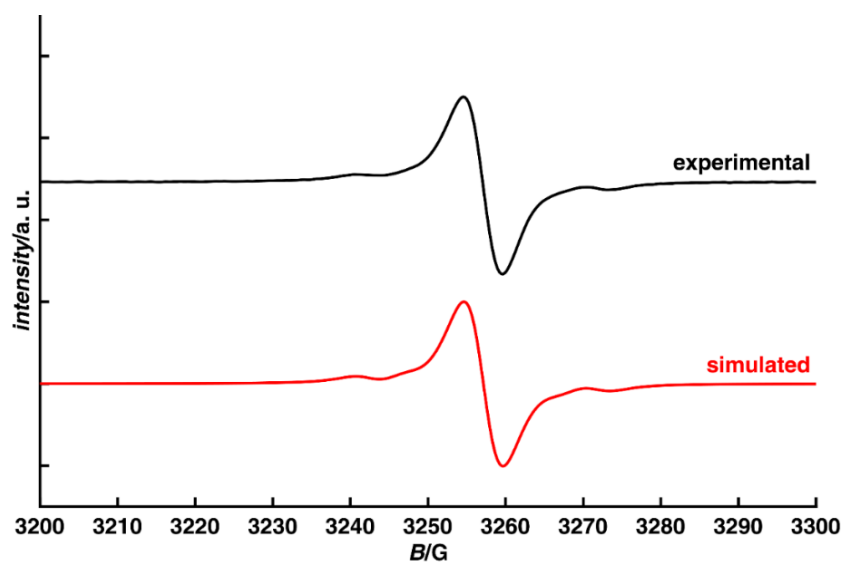


**Fig. S14** X-Band cw-EPR spectra (1:1 C<sub>7</sub>H<sub>8</sub>/CH<sub>2</sub>Cl<sub>2</sub>, 293 K): [MesPd-PCy<sub>3</sub>]N(SO<sub>2</sub>CF<sub>3</sub>)<sub>2</sub>, microwave frequency = 9.293992 GHz, microwave power = 0.0317 mW, modulation amplitude = 0.0702 mT, Simulated parameters:  $g_{\text{iso}} = 2.039$ ,  $A_{\text{iso}}(^{105}\text{Pd}) = 17$  MHz; full line width at half maximum (Gaussian; Lorentzian)  $lw = [0.293; 0.634]$  mT.

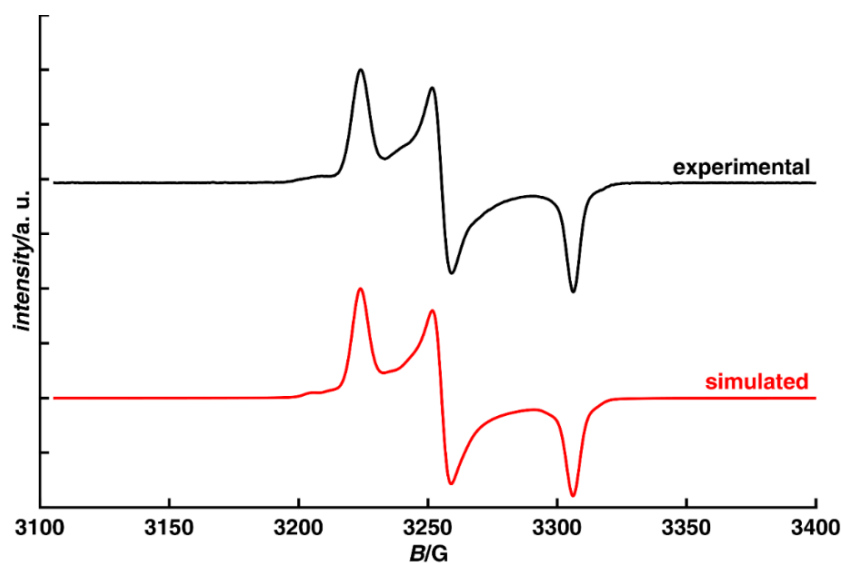


**Fig. S15** X-Band cw-EPR spectra (1:1 C<sub>7</sub>H<sub>8</sub>/CH<sub>2</sub>Cl<sub>2</sub>, 110 K): [MesPd-PCy<sub>3</sub>]N(SO<sub>2</sub>CF<sub>3</sub>)<sub>2</sub>, microwave frequency = 9.305645 GHz, microwave power = 0.1262 mW, modulation amplitude = 0.0701 mT, Simulated parameters:  $g_x = 2.062$ ,  $g_y = 2.042$ ,  $g_z = 2.011$ ,  $A_x(^{105}\text{Pd}) = 22$ ,  $A_y(^{105}\text{Pd}) = 7$ ,  $A_z(^{105}\text{Pd}) = 10$  MHz; full line width at half maximum (Gaussian; Lorentzian)  $lw = [0.526; 0.172]$  mT,  $g\text{Strain} = [0.00197; 0.0006; 0]$ .

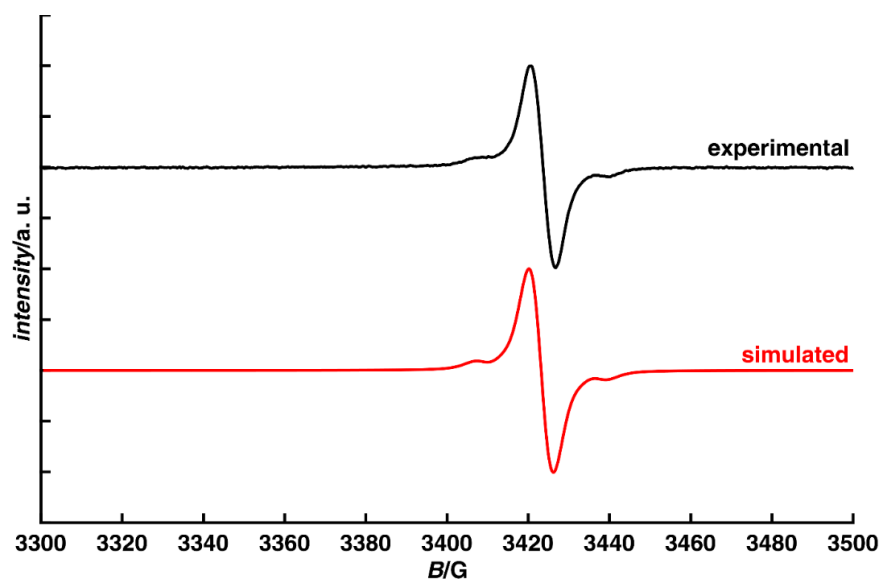


**Fig. S16** X-Band cw-EPR spectra (1:1  $C_7H_8/CH_2Cl_2$ , 293 K):  $[^{Mes}Pd-PPh_3]N(SO_2CF_3)_2$ , microwave frequency = 9.7548510 GHz, microwave power = 2 mW, modulation amplitude = 0.4767 mT, Simulated parameters:  $g_{iso} = 2.036$ ,  $A_{iso}(^{105}Pd) = 16$  MHz; full line width at half maximum (Gaussian; Lorentzian)  $lw = [0.486; 0.535]$  mT.

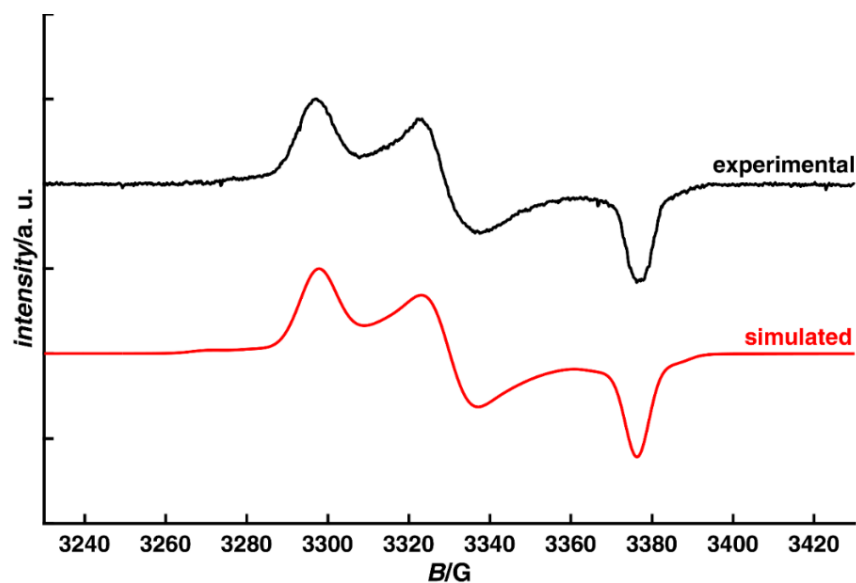


**Fig. S17** X-Band cw-EPR spectra (1:1  $C_7H_8/CH_2Cl_2$ , 77 K):  $[^{Mes}Pd-PPh_3]N(SO_2CF_3)_2$ , microwave frequency = 9.4982505 GHz, microwave power = 2 mW, modulation amplitude = 0.26804 mT, Simulated parameters:  $g_x = 2.058$ ,  $g_y = 2.038$ ,  $g_z = 2.010$ ,  $A_x(^{105}Pd) = 31$ ,  $A_y(^{105}Pd) = 13$ ,  $A_z(^{105}Pd) = 12$  MHz; full line width at half maximum (Gaussian; Lorentzian)  $lw = [0.0683; 0.0857]$  mT,  $gStrain = [0.00625; 0.00711; 0.00385]$ .

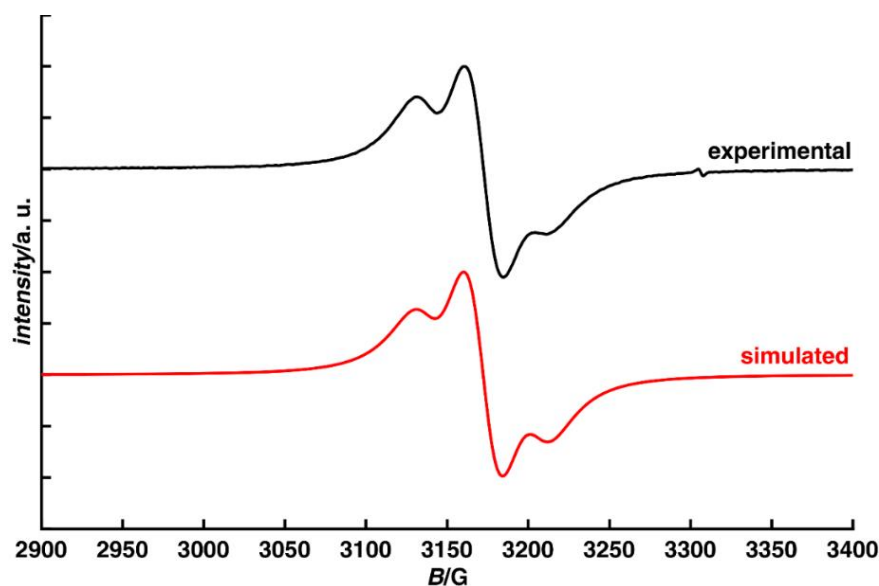


**Fig. S18** X-Band cw-EPR spectra (1:1 C<sub>7</sub>H<sub>8</sub>/CH<sub>2</sub>Cl<sub>2</sub>, 293 K): [MesPt-PCy<sub>3</sub>]N(SO<sub>2</sub>CF<sub>3</sub>)<sub>2</sub>, microwave frequency = 9.297227 GHz, microwave power = 2 mW, modulation amplitude = 0.3 mT, Simulated parameters:  $g_{\text{iso}} = 2.094$ ,  $A_{\text{iso}}(^{195}\text{Pt}) = 192$  MHz; full line width at half maximum (Gaussian; Lorentzian)  $lw = [0.400; 4.501]$  mT.

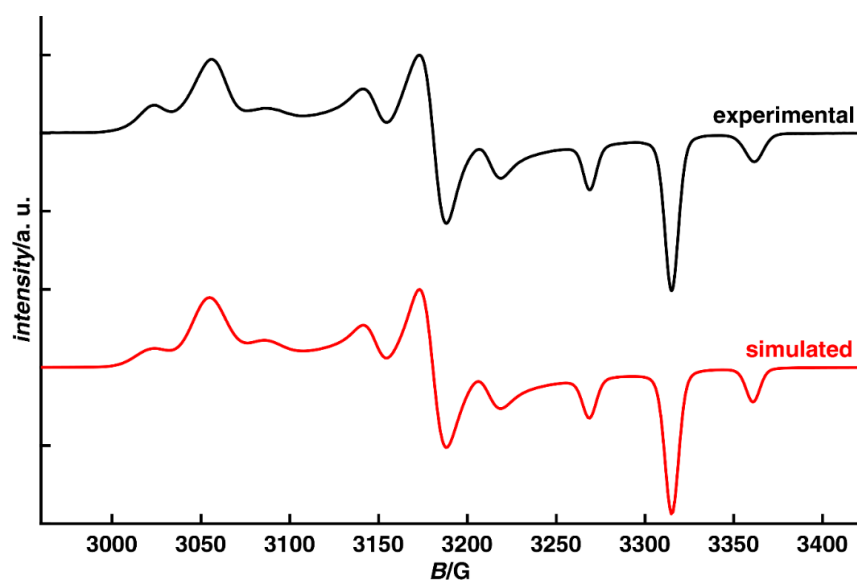


**Fig. S19** X-Band cw-EPR spectra (1:1 C<sub>7</sub>H<sub>8</sub>/CH<sub>2</sub>Cl<sub>2</sub>, 110 K): [MesPt-PCy<sub>3</sub>]N(SO<sub>2</sub>CF<sub>3</sub>)<sub>2</sub>, microwave frequency = 9.306359 GHz, microwave power = 2 mW, modulation amplitude = 0.3 mT, Simulated parameters:  $g_x = 2.177$ ,  $g_y = 2.091$ ,  $g_z = 2.006$ ,  $A_x(^{195}\text{Pt}) = 191$ ,  $A_y(^{195}\text{Pt}) = 186$ ,  $A_z(^{195}\text{Pt}) = 259$  MHz; full line width at half maximum (Gaussian; Lorentzian)  $lw = [0.788; 0.226]$  mT,  $g\text{Strain} = [0.0142; 0.00679; 0]$ .

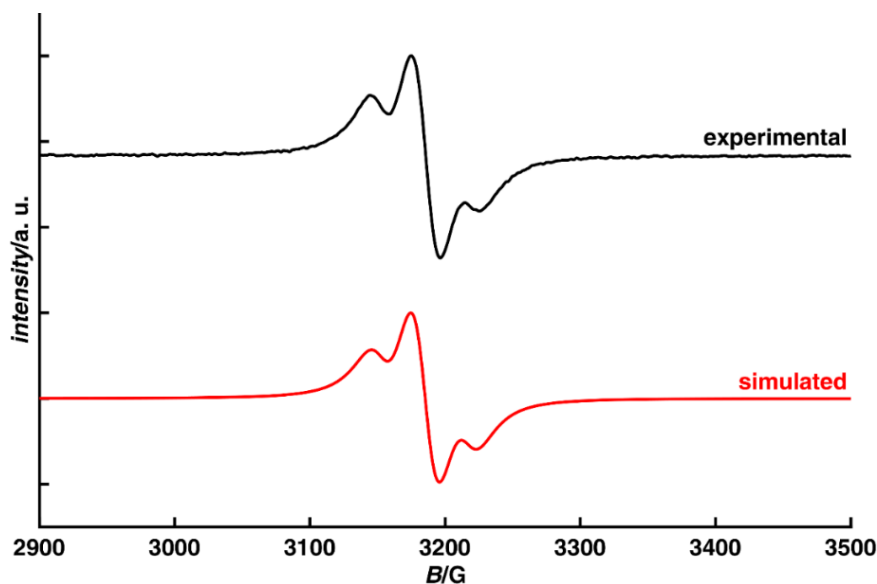


**Fig. S20** X-Band cw-EPR spectra (1:1  $C_7H_8/CH_2Cl_2$ , 293 K):  $[tBuPt-PPh_3]BARF_4$ , microwave frequency = 9.294807 GHz, microwave power = 0.5024 mW, modulation amplitude = 0.2 mT, Simulated parameters:  $g_{iso} = 2.085$ ,  $A_{iso}(^{195}Pt) = 181$  MHz; full line width at half maximum (Gaussian; Lorentzian)  $lw = [0.520; 3.901]$  mT.

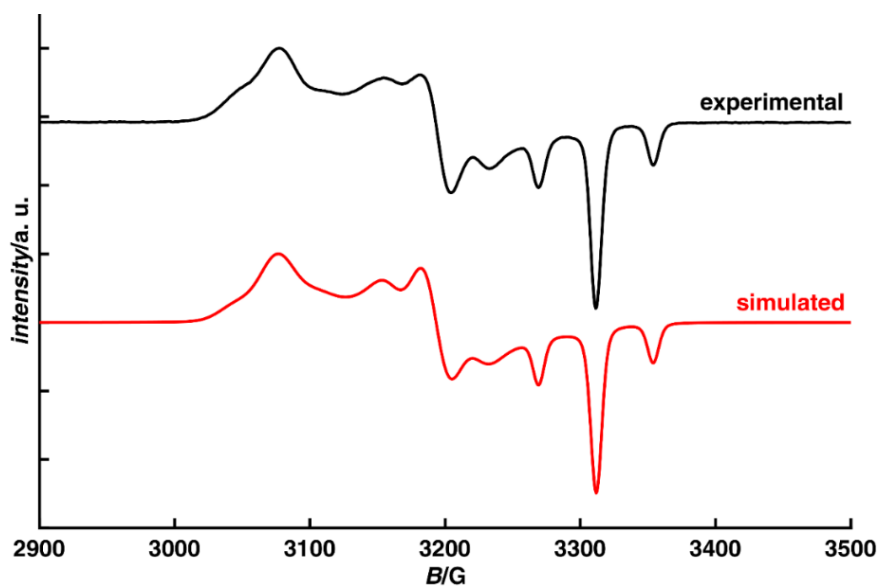


**Fig. S21** X-Band cw-EPR spectra (1:1  $C_7H_8/CH_2Cl_2$ , 110 K):  $[tBuPt-PPh_3]BARF_4$ , microwave frequency = 9.304133 GHz, microwave power = 0.5024 mW, modulation amplitude = 0.2 mT, Simulated parameters:  $g_x = 2.162$ ,  $g_y = 2.082$ ,  $g_z = 2.007$ ,  $A_x(^{195}Pt) = 178$ ,  $A_y(^{195}Pt) = 177$ ,  $A_z(^{195}Pt) = 238$  MHz; full line width at half maximum (Gaussian; Lorentzian)  $lw = [0.766; 0.325]$  mT,  $gStrain = [0.0194; 0.0129; 0.00122]$ .

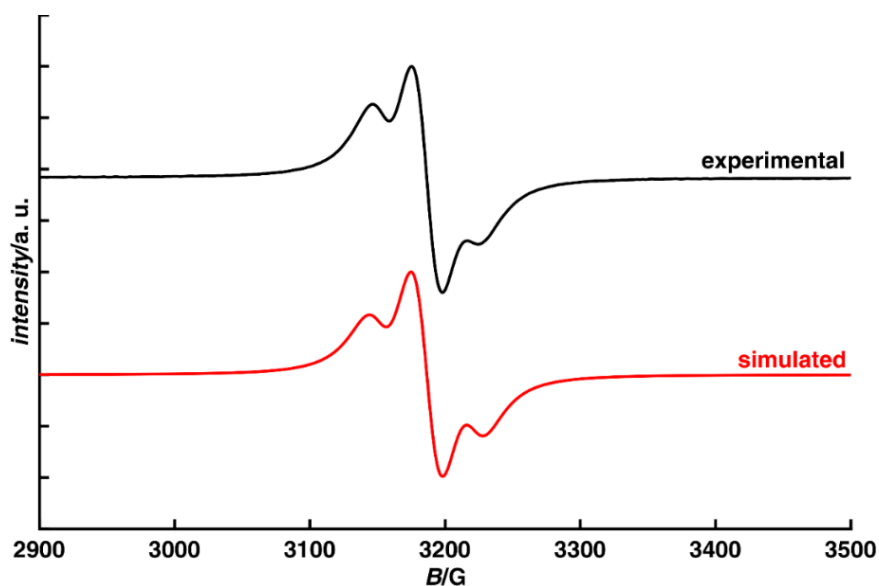


**Fig. S22** X-Band cw-EPR spectra (1:1  $C_7H_8/CH_2Cl_2$ , 293 K):  $[tBuPt-PPh_3]N(SO_2CF_3)_2$ , microwave frequency = 9.295042 GHz, microwave power = 2 mW, modulation amplitude = 0.3 mT, Simulated parameters:  $g_{iso} = 2.084$ ,  $A_{iso}(^{195}Pt) = 195$  MHz; full line width at half maximum (Gaussian; Lorentzian)  $lw = [0.689; 4.221]$  mT.

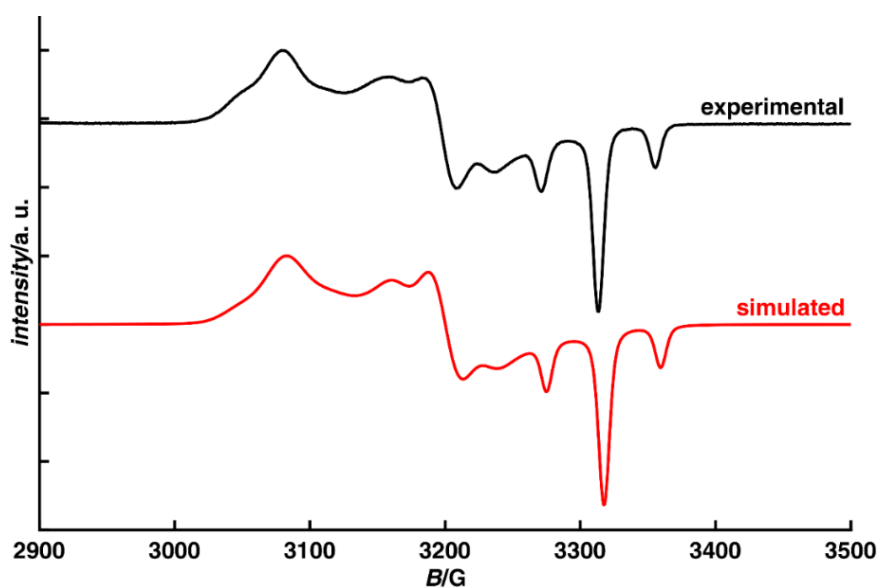


**Fig. S23** X-Band cw-EPR spectra (1:1  $C_7H_8/CH_2Cl_2$ , 123 K):  $[tBuPt-PPh_3]N(SO_2CF_3)_2$ , microwave frequency = 9.304748 GHz, microwave power = 2 mW, modulation amplitude = 0.3 mT, Simulated parameters:  $g_x = 2.158$ ,  $g_y = 2.078$ ,  $g_z = 2.004$ ;  $A_x(^{195}Pt) = 185$ ,  $A_y(^{195}Pt) = 175$ ,  $A_z(^{195}Pt) = 237$  MHz; full line width at half maximum (Gaussian; Lorentzian)  $lw = [0.676; 0.455]$  mT,  $gStrain = [0.0212; 0.0141; 0.000747]$ .

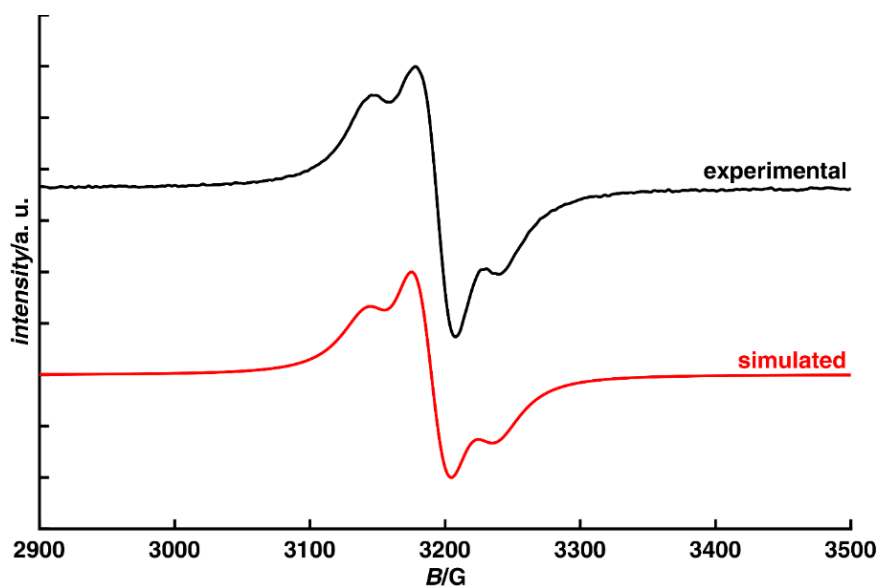


**Fig. S24** X-Band cw-EPR spectra (1:1  $C_7H_8/CH_2Cl_2$ , 293 K):  $[tBuPt-PCy_3]N(SO_2CF_3)_2$ , microwave frequency = 9.293009 GHz, microwave power = 0.5 mW, modulation amplitude = 0.3 mT, Simulated parameters:  $g_{iso} = 2.079$ ;  $A_{iso}(^{195}Pt) = 214$  MHz, full line width at half maximum (Gaussian; Lorentzian)  $lw = [1.415 \ 4.778]$  mT.

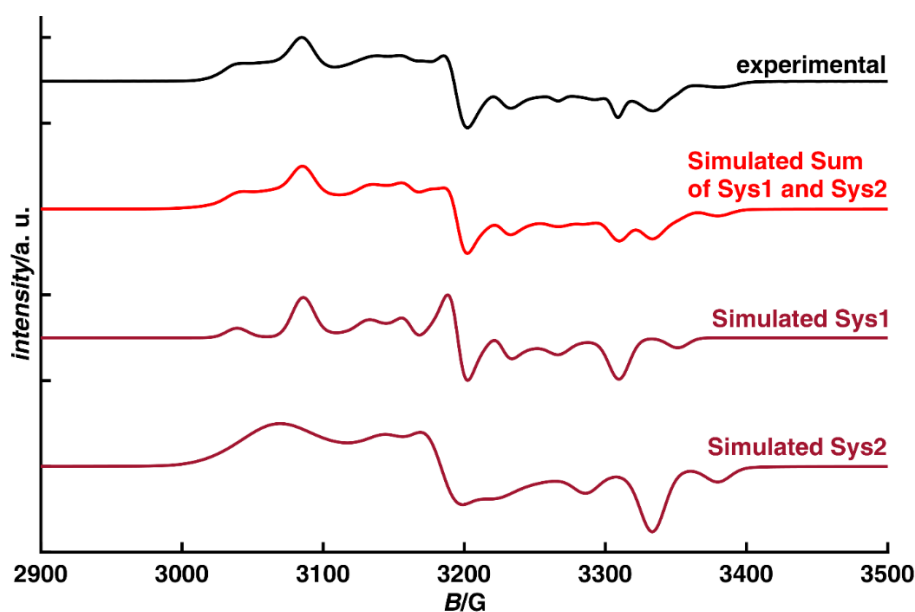


**Fig. S25** X-Band cw-EPR spectra (1:1  $C_7H_8/CH_2Cl_2$ , 123 K):  $[tBuPt-PCy_3]N(SO_2CF_3)_2$ , microwave frequency = 9.306693 GHz, microwave power = 07962 mW, modulation amplitude = 0.3 mT, Simulated parameters for System 1 (Sys1):  $g_x = 2.155$ ,  $g_y = 2.081$ ,  $g_z = 2.009$ ;  $A_x(^{195}Pt) = 280$ ,  $A_y(^{195}Pt) = 189$ ,  $A_z(^{195}Pt) = 237$  MHz; full line width at half maximum (Gaussian; Lorentzian)  $lw = [1.2909; 0]$  mT,  $gStrain = [0.00867; 0.00121; 0.00645]$ , weight = 0.794. Simulated parameters for System 2 (Sys2):  $g_x = 2.169$ ,  $g_y = 2.089$ ,  $g_z = 1.995$ ;  $A_x(^{195}Pt) = 168$ ,  $A_y(^{195}Pt) = 173$ ,  $A_z(^{195}Pt) = 261$  MHz; full line width at half maximum (Gaussian; Lorentzian)  $lw = [1.382; 0.396]$  mT,  $gStrain = [0.0328; 0.0141; 0.00748]$ , weight = 1.432.

## 8 Additional Electrochemical Data

**Table S4** CV data measured in CH<sub>2</sub>Cl<sub>2</sub> at 17 °C in 0.1 M nBu<sub>4</sub>NPF<sub>6</sub>.  $E$ / mV vs. Fc/[Fc]<sup>+</sup>, Fc = ferrocene;  $E(100 \text{ mVs}^{-1})$  for electrochemically quasi- (qr) or irreversible (ir) processes.

	$E^0_1$	$E^0_2$	$\Delta E^0_{1-2}$
<sup>Mes</sup> Ni-PCy <sub>3</sub>	134 (ir)	941 (ir)	807
<sup>Mes</sup> Pd-PCy <sub>3</sub>	172	854	682
<sup>Mes</sup> Pd-PPh <sub>3</sub>	192	728 (ir)	536
<sup>Mes</sup> Pt-PCy <sub>3</sub>	32	806	774
<sup>Mes</sup> Pt-PPh <sub>3</sub> <sup>[a]</sup>	60	727	667
<sup>tBu</sup> Pt-PCy <sub>3</sub>	20	668	648
<sup>tBu</sup> Pt-PPh <sub>3</sub>	72	679 (qr)	607

[a] Data included for comparison from ref. 16.

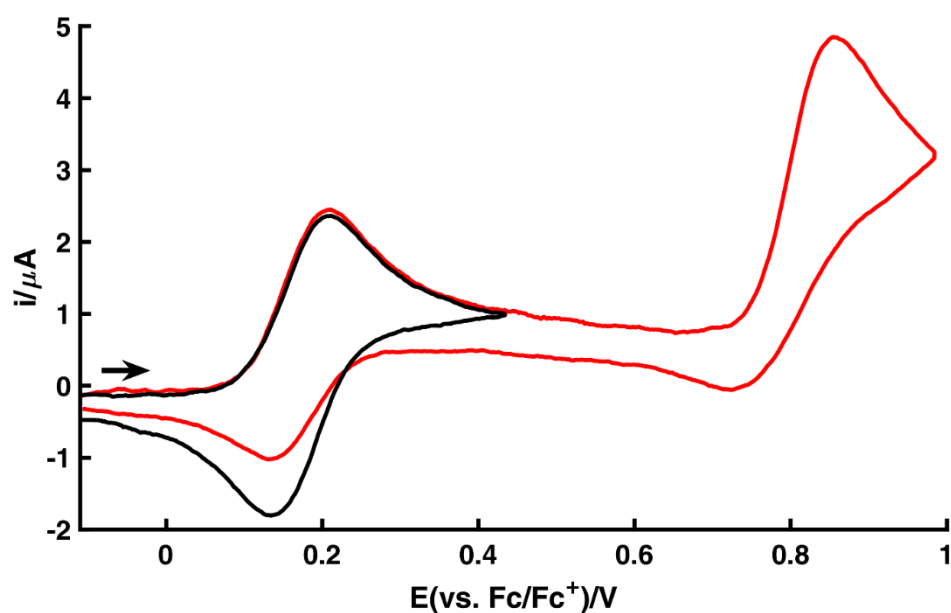


**Fig. S26** CV  $i$ - $E$  curves (0.1 M nBu<sub>4</sub>NPF<sub>6</sub>/CH<sub>2</sub>Cl<sub>2</sub>, 100 mV s<sup>-1</sup>, 17 °C): 0.135mM <sup>Mes</sup>Pd-PCy<sub>3</sub> (black, potential sweep direction reversed at 0.433 V).

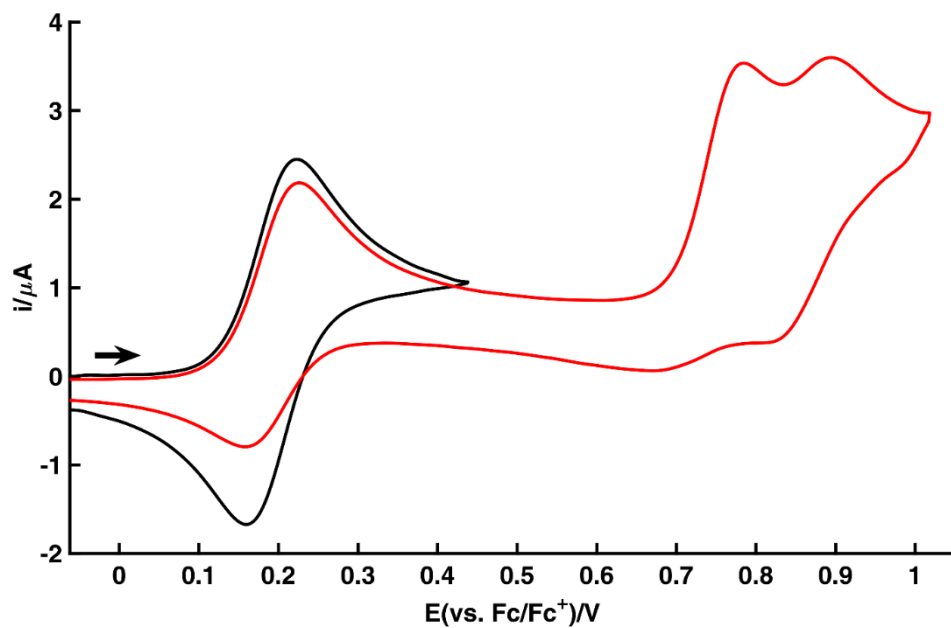


**Fig. S27** CV *i-E* curves (0.1 M nBu<sub>4</sub>NPF<sub>6</sub>/CH<sub>2</sub>Cl<sub>2</sub>, 100 mV s<sup>-1</sup>, 17 °C): 0.093 mM <sup>Mes</sup>Pd-PPh<sub>3</sub> (red); 0.086 mM <sup>Mes</sup>Pd-PPh<sub>3</sub> (black, potential sweep direction reversed at 0.44 V).

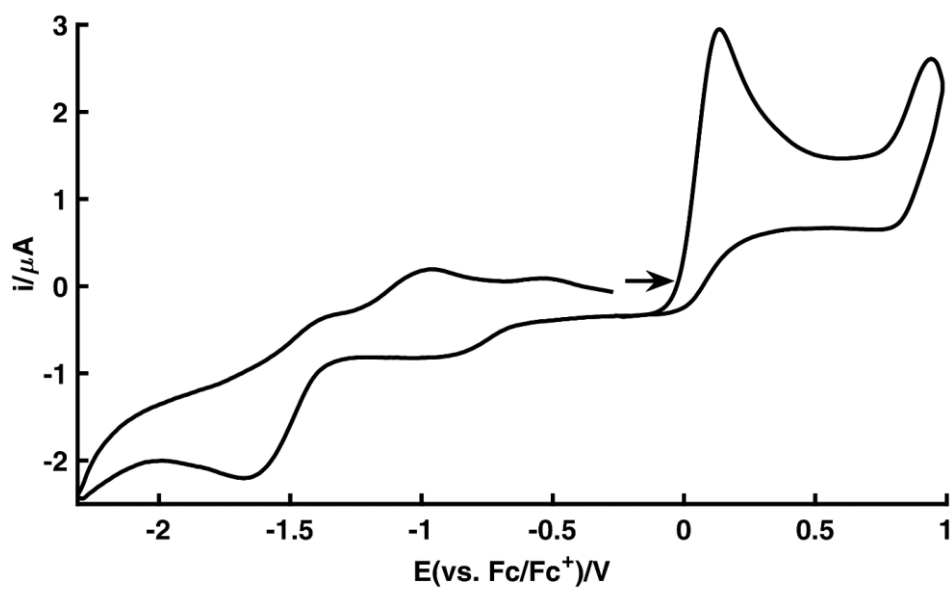


**Fig. S28** CV *i-E* curves (0.1 M nBu<sub>4</sub>NPF<sub>6</sub>/CH<sub>2</sub>Cl<sub>2</sub>, 100 mV s<sup>-1</sup>, 17 °C): 0.06 mM <sup>Mes</sup>Ni-PCy<sub>3</sub>.

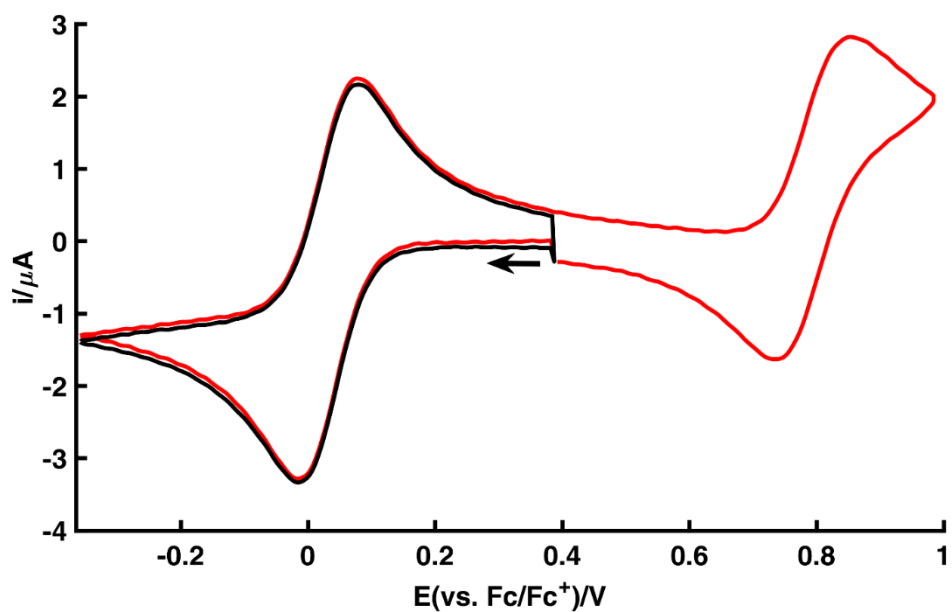


**Fig. S29** CV  $i$ - $E$  curves (0.1 M  $n\text{Bu}_4\text{NPF}_6/\text{CH}_2\text{Cl}_2$ ,  $100 \text{ mV s}^{-1}$ ,  $17 \text{ }^\circ\text{C}$ ): 0.182 mM  $[\text{MesPt-PCy}_3]\text{N}(\text{SO}_2\text{CF}_3)_2$  (black, potential sweep finished at 0.39 V).

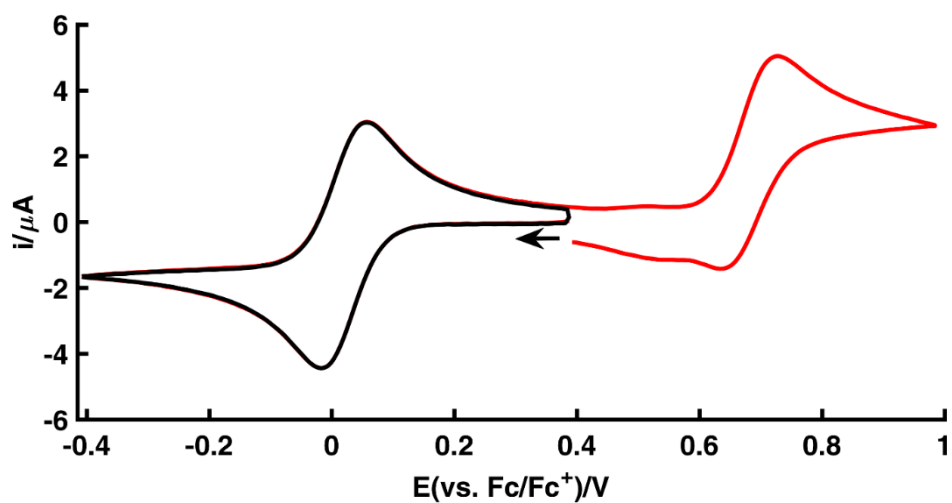


**Fig. S30** CV  $i$ - $E$  curves (0.1 M  $n\text{Bu}_4\text{NPF}_6/\text{CH}_2\text{Cl}_2$ ,  $100 \text{ mV s}^{-1}$ ,  $17 \text{ }^\circ\text{C}$ ): 0.213 mM  $[\text{tBuPt-PCy}_3]\text{N}(\text{SO}_2\text{CF}_3)_2$  (black, potential sweep finished at 0.39 V).

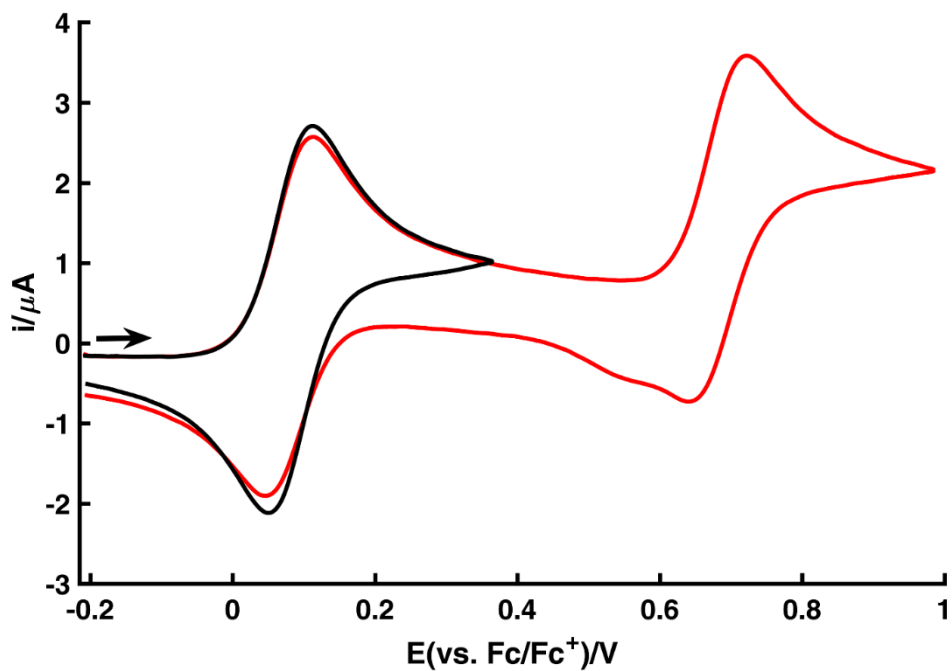


Fig. S31 CV  $i$ - $E$  curves (0.1 M  $n\text{Bu}_4\text{NPF}_6/\text{CH}_2\text{Cl}_2$ ,  $100 \text{ mV s}^{-1}$ ,  $17 \text{ }^\circ\text{C}$ ):  $0.135 \text{ mM } t\text{BuPt-PPh}_3$  (black, potential sweep direction reversed at  $0.37 \text{ V}$ ).

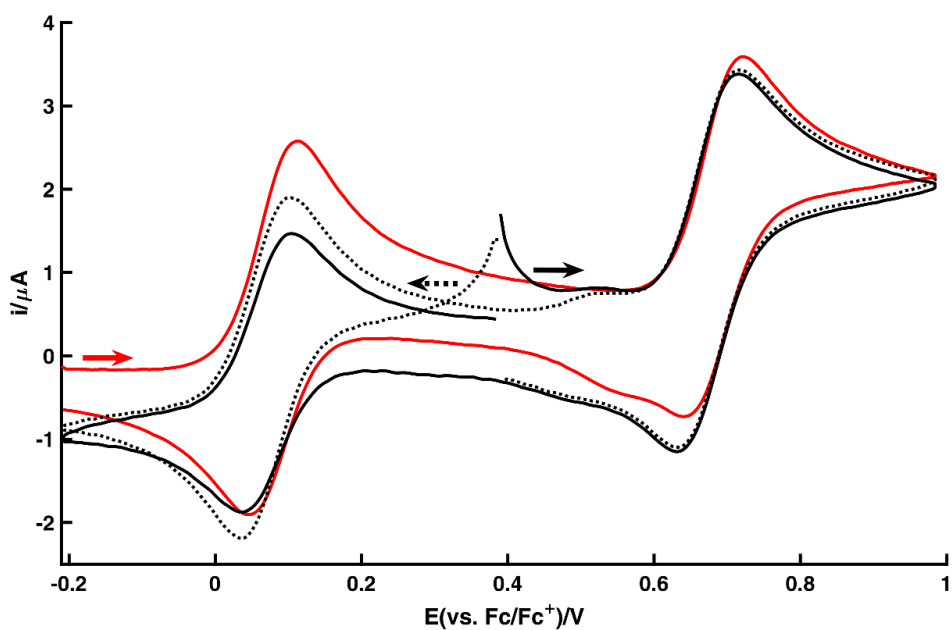


Fig. S32 CV  $i$ - $E$  curves (0.1 M  $n\text{Bu}_4\text{NPF}_6/\text{CH}_2\text{Cl}_2$ ,  $100 \text{ mV s}^{-1}$ ,  $17 \text{ }^\circ\text{C}$ ):  $0.135 \text{ mM } t\text{BuPt-PPh}_3$  (red), and  $0.189 \text{ mM } [t\text{BuPt-PPh}_3]\text{N}(\text{SO}_2\text{CF}_3)_2$  (black, solid and dashed).

## 9 Additional Computational Data

### 9.1 General Information

All calculations were performed using the ADF2017.111 release<sup>31, 32</sup> or ORCA version 4.0.1<sup>33</sup>.

Structures optimization and EPR calculations were done in ADF, electronic excitations were computed using ORCA. Structures were optimized using the PBE0-1/3-D3(BJ) functional (using the PBE0-D3(BJ) parameter for the dispersion correction and 33.333 % exact exchange) and PBE0-D3(BJ) for the Nickel compound, ZORA and the ZORA-TZP basis set. All property calculations (EPR parameters, TD-DFT) were performed on the PBE0-1/3 level of theory. All ADF calculations used COSMO with the parameters for CH<sub>2</sub>Cl<sub>2</sub> ( $\epsilon = 8.93$ ,  $R_{\text{solv}} = 2.94$ ), a “good” numerical quality. The convergence criteria were set to  $5e-7$  for the commutator of Fock and density matrix in the SCF and to  $1e-5$  hartree for energy change and  $1e-4$  hartree/bohr for gradient change in the structure optimization. EPR parameters were calculated using the collinear ZORA(SO) approach, the ZORA-TZ2P basis set and a Gaussian nuclear model.

Symmetrised non-equilibrium structures to approximately model the transition states for thermal electron transfer from one to the other thiophenolate ligand side were obtained at the same level of theory by symmetrizing the molecular structure and enforcing  $C_s$  symmetry throughout the optimization.

For the TD-DFT calculations, a CPCM model with the COSMO  $f(\epsilon)$  and the parameters used in ADF and ZORA were used. The calculations employed the ZORA-def2-TZVPP basis sets from the internal ORCA library (old-ZORA-TZVPP for Pd and SARC-ZORA-TZVPP for Pt), the RIJCOSX approximation with the “AutoAux” function for the fitting basis sets and the “VeryTightSCF” convergence criteria, as well as a Grid5 grid and a GridX6 COSX-grid. In the TD-DFT part, 50 roots were converged. The oscillator strengths given in the main text were obtained via the transition electric dipole moment route.

Due to convergence problems, the calculation on the symmetric structures were performed in  $C_1$  symmetry as well. Inspection of the Mulliken spin populations confirmed a symmetric electronic structure. Comparison with NPA charges established that the wavefunctions in both programs were comparable.

## 9.2 Computational Results

**Table S5** Comparison of calculated EPR parameters and TD-DFT data.

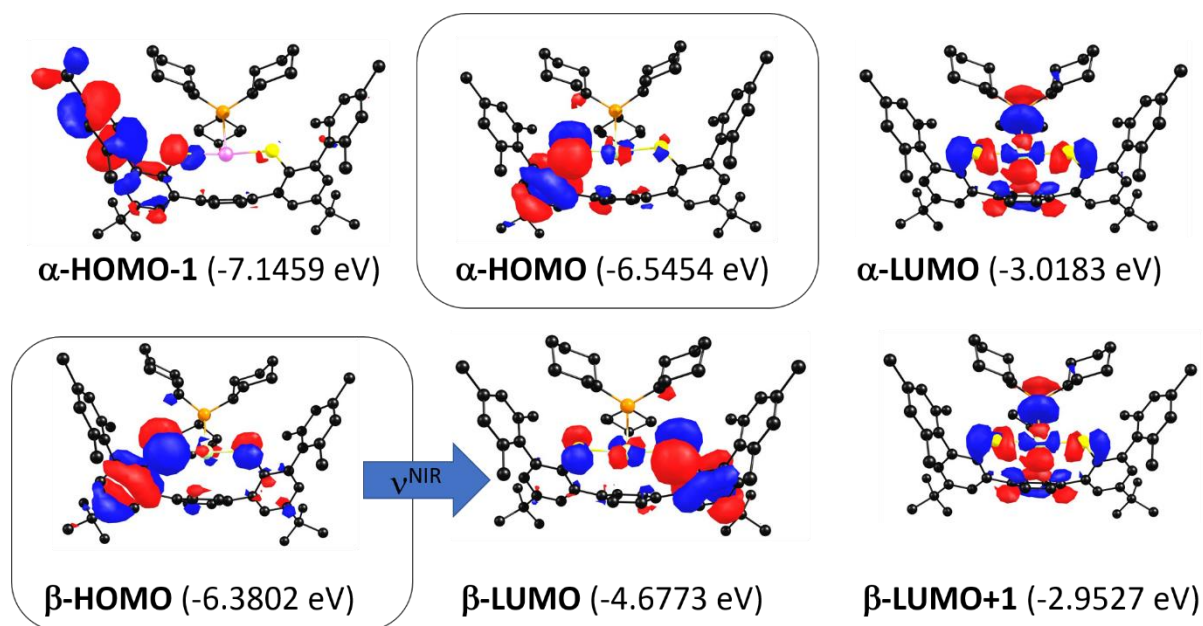
	PBE0-1/3		
	$[\text{MesNi-PCy}_3]^+$	$[\text{MesPd-PCy}_3]^+$	$[\text{MesPt-PCy}_3]^+$
$g_{\text{iso}}^{\text{a)}$	2.054	2.038	2.099
$\Delta g^{\text{a)}$	0.263	0.062	0.174
$A_{\text{iso}}/\text{MHz}$	3	15	183
$\lambda^{\text{NIR}}/\text{nm}$	1790	1800	1260
$\nu^{\text{NIR}}/\text{cm}^{-1}$	5570	5540	7910
$f_{\text{osc}}$	0.125	0.103	0.238

$$\text{a) } g_{\text{iso}} = 1/3 \times (g_{\text{xx}} + g_{\text{yy}} + g_{\text{zz}}), \Delta g = g_{\text{xx}} - g_{\text{zz}}$$

**Table S6** Comparison of minimum and symmetrized non-equilibrium structures.

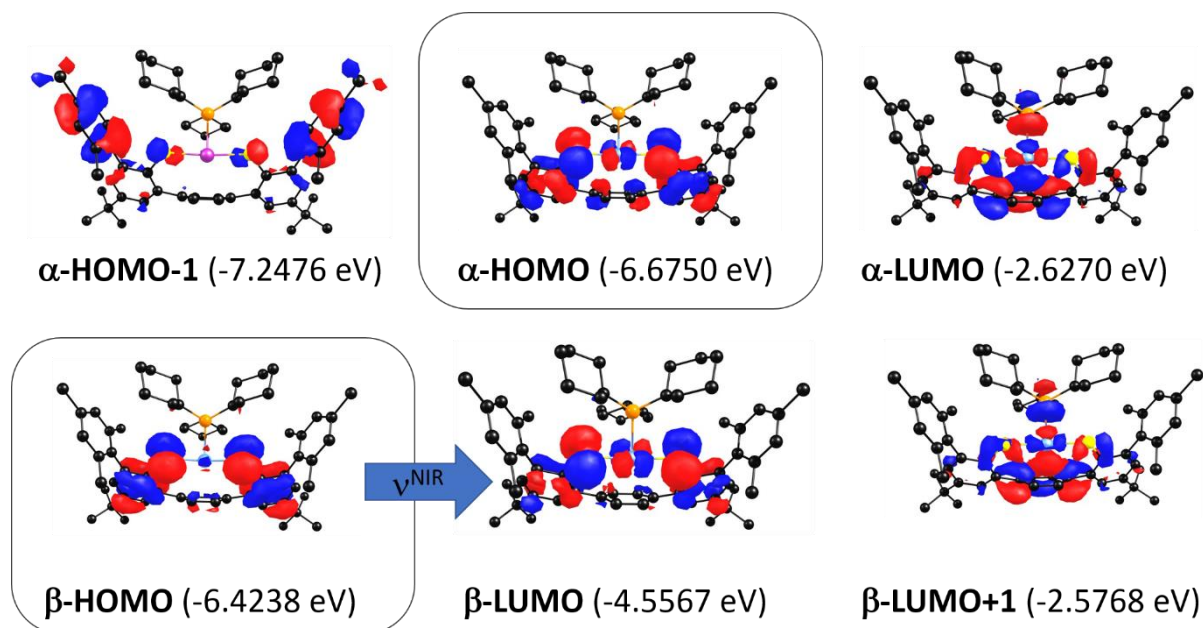
	PBE0-1/3				
	$[\text{MesNi-PCy}_3]^+$	$[\text{MesNi-PCy}_3]^+$	$[\text{MesPd-PCy}_3]^+$	$[\text{MesPd-PCy}_3]^+$	$[\text{MesPt-PCy}_3]^+$
	$C_s$ symmetry <sup>a)</sup>		$C_s$ symmetry <sup>b)</sup>		
d(M-S)/Å	2.177/2.185	2.183	2.319/2.333	2.317	2.304/2.306
d(Ar-S)/Å	1.759/1.757	1.758	1.762/1.722	1.743	1.749/1.748
$\nu^{\text{NIR}}/\text{cm}^{-1}$	5570	5525	5540	5875	7910
$f_{\text{osc}}$	0.125	0.127	0.103	0.188	0.238
spin populations <sup>c)</sup>					
S/S'	0.246/0.281	0.259/0.272	0.093/0.542	0.311/0.320	0.317/0.324
M	0.298	0.288	0.064	0.079	0.115

<sup>a)</sup> 1 kJ/mol above equilibrium ground state configuration. <sup>b)</sup> 1 kJ/mol below equilibrium ground state configuration. <sup>c)</sup> Mulliken spin populations.



Contour value of isosurfaces (neg. = blue, pos. = red) = 0.0333.

**Fig. S33** Kohn-Sham MOs and energies for  $[\text{MesPd-PCy}_3]^+$  from a spin-unrestricted BPE0-1/3-D3(BJ)/ZORA DFT calculation. TD-DFT derived lowest-energy transition ( $\beta\text{HOMO} \rightarrow \beta\text{LUMO}$ ):  $\lambda^{\text{NIR}}(\text{computed}) = 1800 \text{ nm}$  ( $5560 \text{ cm}^{-1}$ ).



Contour value of isosurfaces (neg. = blue, pos. = red) = 0.0333.

**Fig. S34** Kohn-Sham MOs and energies for  $[\text{MesPt-PCy}_3]^+$  from a spin-unrestricted BPE0-1/3-D3(BJ)/ZORA DFT calculation. TD-DFT derived lowest-energy transition ( $\beta\text{HOMO} \rightarrow \beta\text{LUMO}$ ):  $\lambda^{\text{NIR}}(\text{computed}) = 1260 \text{ nm}$  ( $7940 \text{ cm}^{-1}$ ).

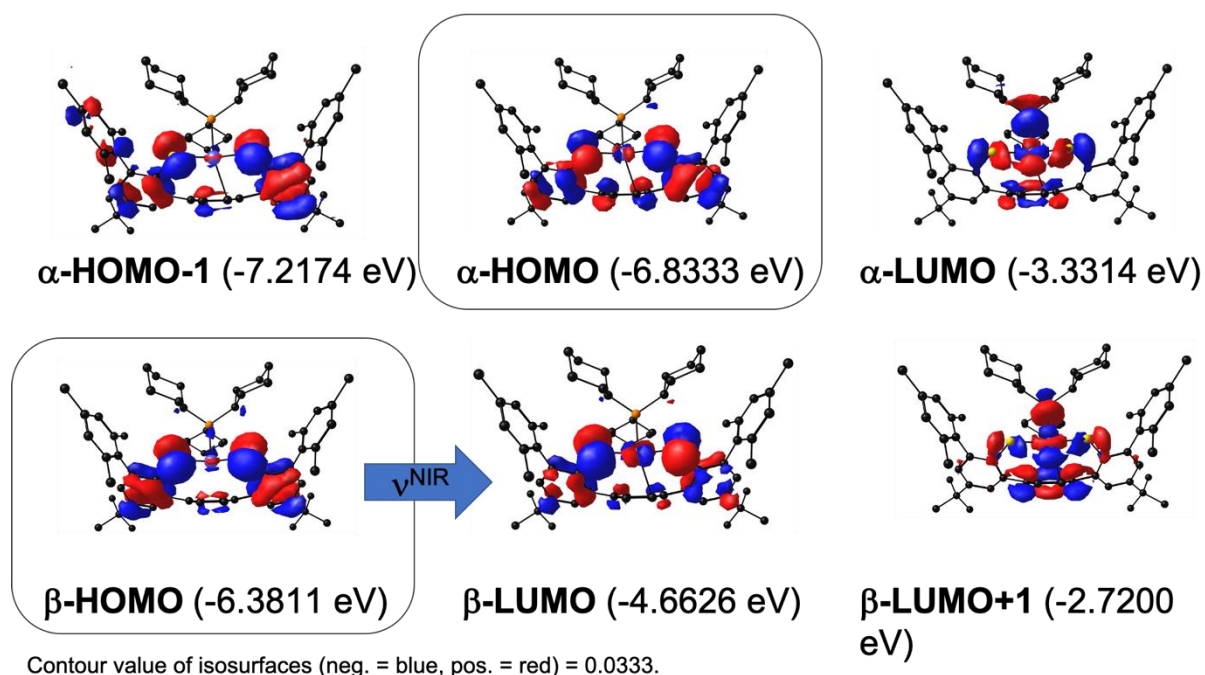


**Fig. S35** Kohn-Sham MOs and energies for  $[\text{MesNi-PCy}_3]^+$  from a spin-unrestricted BPE0-1/3-D3(BJ)/ZORA DFT calculation. TD-DFT derived lowest-energy transition ( $\beta\text{HOMO} \rightarrow \beta\text{LUMO}$ ):  $\lambda^{\text{NIR}}(\text{computed}) = 1795 \text{ nm}$  ( $5570 \text{ cm}^{-1}$ ).

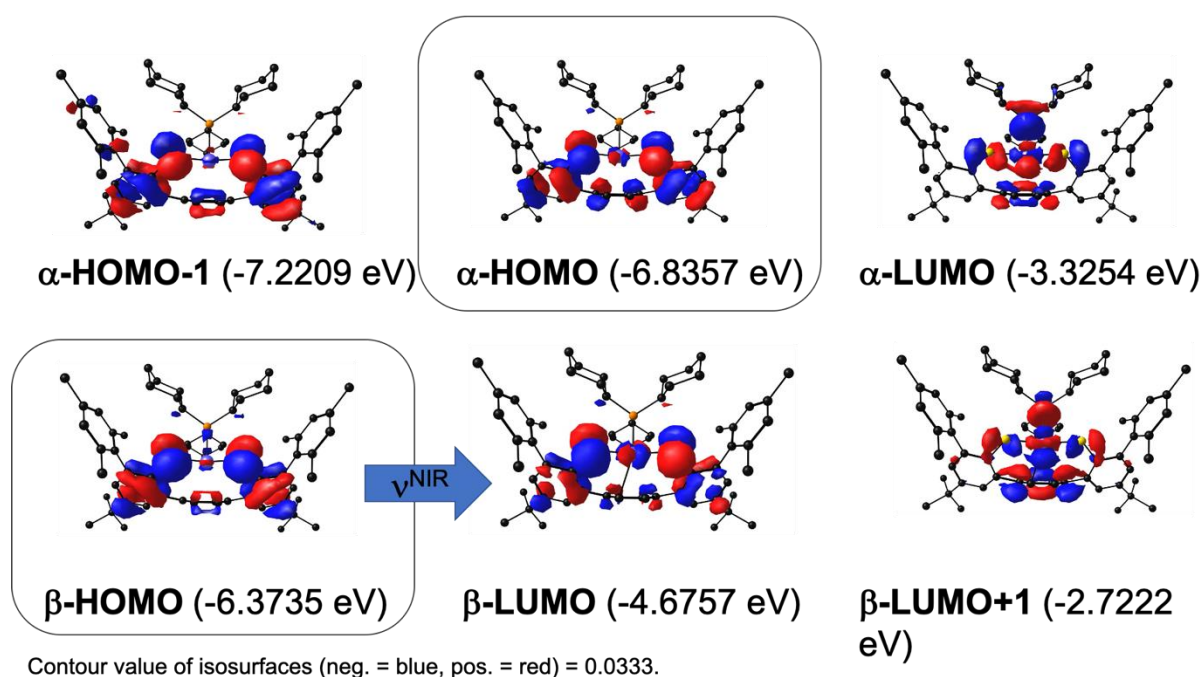


**Fig. S36** Kohn-Sham MOs and energies for  $[\text{MesNi-PCy}_3]^+$  from a spin-unrestricted BPE0-1/3-D3(BJ)/ZORA DFT calculation using a  $C_s$  symmetric structure. TD-DFT derived lowest-energy transition ( $\beta\text{HOMO} \rightarrow \beta\text{LUMO}$ ):  $\lambda^{\text{NIR}}(\text{computed}) = 1810 \text{ nm}$  ( $5525 \text{ cm}^{-1}$ ).

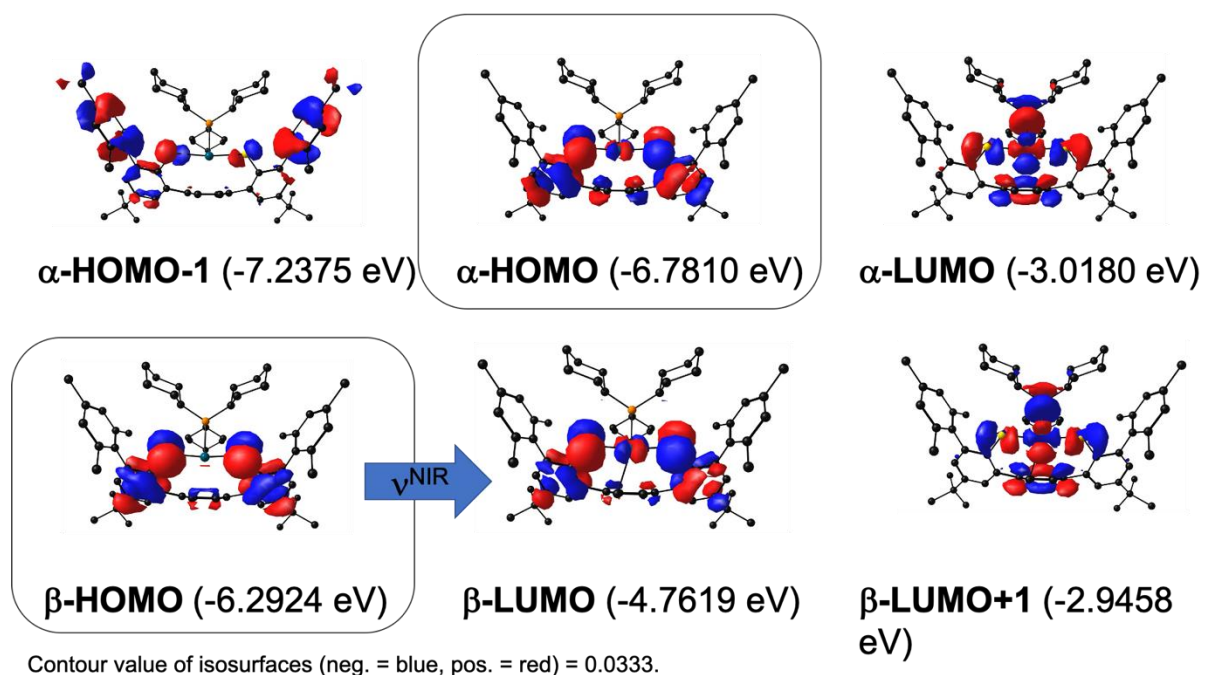


**Fig. S37** Kohn-Sham MOs and energies for  $[\text{MesPd-PCy}_3]^+$  from a spin-unrestricted BPE0-1/3-D3(BJ)/ZORA DFT calculation using a  $C_s$  symmetric structure. TD-DFT derived lowest-energy transition ( $\beta$ HOMO  $\rightarrow$   $\beta$ LUMO):  $\lambda^{\text{NIR}}(\text{computed}) = 1700 \text{ nm}$  ( $5875 \text{ cm}^{-1}$ ).

## 10 References

1. D. Herebian, E. Bothe, F. Neese, T. Weyhermüller and K. Wieghardt, *J. Am. Chem. Soc.*, 2003, **125**, 9116-9128.
2. D. Herebian, E. Bothe, E. Bill, T. Weyhermüller and K. Wieghardt, *J. Am. Chem. Soc.*, 2001, **123**, 10012-10023.
3. K. Ray, T. Weyhermüller, F. Neese and K. Wieghardt, *Inorg. Chem.*, 2005, **44**, 5345-5360.
4. K. M. Conner, A. L. Perugini, M. Malabute and S. N. Brown, *Inorg. Chem.*, 2018, **57**, 3272-3286.
5. P. Chaudhuri, C. N. Verani, E. Bill, E. Bothe, T. Weyhermüller and K. Wieghardt, *J. Am. Chem. Soc.*, 2001, **123**, 2213-2223.
6. X. Sun, H. Chun, K. Hildenbrand, E. Bothe, T. Weyhermüller, F. Neese and K. Wieghardt, *Inorg. Chem.*, 2002, **41**, 4295-4303.
7. S. Kokatam, T. Weyhermüller, E. Bothe, P. Chaudhuri and K. Wieghardt, *Inorg. Chem.*, 2005, **44**, 3709-3717.
8. N. Leconte, J. Moutet, T. Constantin, F. Molton, C. Philouze and F. Thomas, *Eur. J. Inorg. Chem.*, 2018, **2018**, 1752-1761.
9. R. Kunert, C. Philouze, O. Jarjayes and F. Thomas, *Inorg. Chem.*, 2019, **58**, 8030-8044.
10. Y. Shimazaki, T. D. Stack and T. Storr, *Inorg. Chem.*, 2009, **48**, 8383-8392.
11. Y. Shimazaki, T. Yajima, F. Tani, S. Karasawa, K. Fukui, Y. Naruta and O. Yamauchi, *J. Am. Chem. Soc.*, 2007, **129**, 2559-2568.
12. Y. Shimazaki, N. Arai, T. J. Dunn, T. Yajima, F. Tani, C. F. Ramogida and T. Storr, *Dalton Trans.*, 2011, **40**, 2469-2479.
13. F. Koch, H. Schubert, P. Sirsch and A. Berkefeld, *Dalton Trans.*, 2015, **44**, 13315-13324.
14. G. B. Kauffman, D. O. Cowan, G. Slusarczuk and S. Kirschner, in *Inorg. Synth.*, ed. J. Kleinberg, John Wiley & Sons, Inc., Hoboken, NJ, USA, 1963, vol. 7, ch. cis- and trans-Dichlorodiammineplatinum(II), pp. 239-245.
15. H. D. K. Drew, F. W. Pinkard, G. H. Preston and W. Wardlaw, *J. Chem. Soc.*, 1932, DOI: 10.1039/jr9320001895, 1895-1909.
16. N. M. Mews, A. Berkefeld, G. Hörner and H. Schubert, *J. Am. Chem. Soc.*, 2017, **139**, 2808-2815.
17. S. V. Rosokha, C. L. Stern and J. T. Ritzert, *CrystEngComm*, 2013, **15**.
18. M. Schlosser and J. Hartmann, *Angew. Chem. Int. Ed. Engl.*, 1973, **12**, 508-509.
19. F. Koch, A. Berkefeld, H. Schubert and C. Grauer, *Chem. Eur. J.*, 2016, **22**, 14640-14647.
20. S. Stoll and A. Schweiger, *J Magn Reson*, 2006, **178**, 42-55.
21. F. Murrieta-Guevara and A. Trejo Rodriguez, *Journal of Chemical & Engineering Data*, 1984, **29**, 204-206.
22. J. G. Speight, in *Lange's Handbook of Chemistry*, ed. J. G. Speight, McGraw-Hill Education, New York, Chicago, San Francisco, Lisbon, London, Madrid, Mexico City, Milan, New Delhi, San Juan, Seoul, Singapore, Sydney, Toronto, 16. edn., 2005, pp. 2.470-494.
23. D. F. Evans, *J. Chem. Soc.*, 1959, DOI: 10.1039/jr9590002003.
24. G. A. Bain and J. F. Berry, *J. Chem. Educ.*, 2008, **85**.
25. L. J. Farrugia, *J. Appl. Cryst.*, 1999, **32**, 837-838.
26. G. M. Sheldrick, *Acta Crystallographica Section A: Foundations and Advances* 2008, **64**, 112-122.
27. C. B. Hubschle, G. M. Sheldrick and B. Dittrich, *J Appl Crystallogr*, 2011, **44**, 1281-1284.
28. A. L. Spek, *Acta Crystallographica Section D Biological Crystallography*, 2009, **65**, 148-155.
29. L. J. Farrugia, *J. Appl. Cryst.*, 2012, **45**, 849-854.
30. J. Janisch, A. Ruff, B. Speiser, C. Wolff, J. Zigelli, S. Benthin, V. Feldmann and H. A. Mayer, *J. Solid State Electrochem.*, 2011, **15**, 2083-2094.

31. G. te Velde, F. M. Bickelhaupt, E. J. Baerends, C. Fonseca Guerra, S. J. A. van Gisbergen, J. G. Snijders and T. Ziegler, *J. Comput. Chem.*, 2001, **22**, 931-967.
32. C. Fonseca Guerra, J. G. Snijders, G. te Velde and E. J. Baerends, *Theor. Chem. Acc.*, 1998, **99**, 391-403.
33. F. Neese, *WIREs Comput. Mol. Sci.*, 2012, **2**, 73-78.